Detonations in Hydrocarbon Fuel Blends

J.M. Austin and J.E. Shepherd

Graduate Aeronautical Laboratories,
California Institute of Technology
Pasadena, California 91125

Explosion Dynamics Laboratory Report FM99-6
July 10, 2000

Prepared for the Air Force and Advanced Projects Research Inc.,
under contract F04611-98-C-0046

Abstract

A study of detonations in high molecular weight hydrocarbon fuels was performed in two GALCIT facilities: the 280 mm gaseous detonation tube (GDT) and a 1180 liter vessel (HYJET) with jet initiation capability.

In the GDT, detonation pressure, wave speed and cell width measurements were made in hexane-oxygen-nitrogen mixtures with and without the addition of lower molecular weight fuels. Stoichiometric mixtures of hexane-oxygen were studied with nitrogen dilution varying from fuel-oxygen to fuel-air. Hexane-air mixtures were investigated with varying fractions of lower molecular weight fuels (hydrogen, acetylene, ethylene, and carbon monoxide). The measured cell width decreased indicating increased sensitivity to detonation with increasing fraction of hydrogen, acetylene, and ethylene, in order of effectiveness. The addition of a small fraction of carbon monoxide produced a small decrease in the cell width, but addition of more than about 75 % (by fuel mass) carbon monoxide resulted in a rapid increase in cell width.

As the oxidation of carbon monoxide is extremely sensitive to the presence of hydrogenous species, cell width measurements were made in carbon monoxide-air mixtures with the addition of hydrogen or hydrocarbons of various H-atom content and structure (acetylene, ethylene, and hexane). A detonation could be initiated in mixtures with very small fraction of hexane (0.07% of the mixture volume). Cell width measurements were compared to calculated ZND reaction zone parameters, including temperature and radical species concentrations. It was determined that for addition of hydrogen, ethylene or hexane, the cell width can be correlated with the product of the peak OH and CO concentrations in the reaction zone. Mixtures containing acetylene also showed the same linear dependance on this parameter, but, for the same peak OH and CO concentration, the cell widths were a factor of two smaller than those of the other mixtures.

A fuel blend representative of thermally decomposed JP-10 was studied at 295 K. This blend consisted of hydrogen, carbon monoxide, methane, acetylene, ethylene, and hexane with varying fractions of oxygen and nitrogen. The cell width for stoichiometric fuel blend-oxygen was found to be an order of magnitude smaller than that for fuel blend-air. The cell width for the fuel blend-air mixture was about half that of hexane-air.

Further experiments were carried out in the HYJET facility. A hydrogen-oxygen-nitrogen jet was used to initiate detonations in vapor phase mixtures

of hexane (at 295 K) and of dodecane (at 380 K) with stoichiometric oxygen. Pressure and wave speed measurements were made. A critical nitrogen dilution limit was determined for each fuel. The critical limit was found to be $2.5 \leq \beta \leq 3.0$ for hexane, where β is the ratio of nitrogen to oxygen concentration. This corresponds to a D/λ (nozzle diameter/cell width) ratio of 4, which compares well with the value 4.3 previously determined for this driver. The critical nitrogen dilution limit for dodecane was also found to be $2.5 \leq \beta \leq 3.0$. No cell width measurements are currently available for dodecane.

An attempt was made to initiate detonation in a dodecane spray. Pressure and velocity measurements were made and clearly show that no detonation could be directly initiated. Different fuel injection systems were tried and the initial temperature of the mixture was varied.

Contents

List of Figures

List of Tables

Part I
Sensitization of High Molecular Weight Hydrocarbons

1 Introduction

Liquid hydrocarbons are the fuel of choice for aviation propulsion systems, including the pulse detonation engine (PDE) concept. Much of the published PDE research carried out up to the present time has used gaseous fuels, C_1-C_3 hydrocarbons, due to the difficulty of creating uniform fuel-air mixtures with liquid hydrocrabon fuels and initiating these mixtures. The present investigation is part of a larger study that considers how liquid fuels can best be utilized in PDEs. This report describes measurements of detonation properties of fuel-blends that are representative of what might be derived by processing liquid hydrocarbon fuels such as JP-10 and Jet-A.

Liquid fuels have obvious storage advantages over gaseous fuels, but tend to be composed of larger, heavier molecules (C_6 to C_{12}) and are more difficult to detonate than gaseous fuels such as C_1-C_2. A liquid hydrocarbon fuel can be partially decomposed into smaller molecules (C_1 to C_5) by fuel-rich combustion or by thermal cracking. Fuel-rich catalytic combustion uses the presence of a catalyst to achieve combustion beyond the rich combustion limit, producing reactive molecules, high temperatures and little soot. Catalytic combustion of JP-10 was studied by Brabbs and Merritt (1993) in an effort to find a storable liquid fuel which had an ignition delay time that was less than the residence time in the combustion chamber of a hypersonic vehicle. The majority of the combustion products were low-molecular-weight hydrocarbons that are also more susceptible to detonation, making this process an attractive possibility for PDE fuels.

Smaller molecular weight products may act as 'sensitizers' to the parent fuel: reducing the critical energy required to initiate a detonation compared to the parent fuel. The aim of this portion of the study is to investigate the effectiveness of sensitizers on some liquid hydrocarbon fuels by measuring the characteristic cell width of the detonation wave. The cell width is often used to characterize the detonability of a mixture and can be empirically related to parameters such as critical initiation energy, critical diameter or

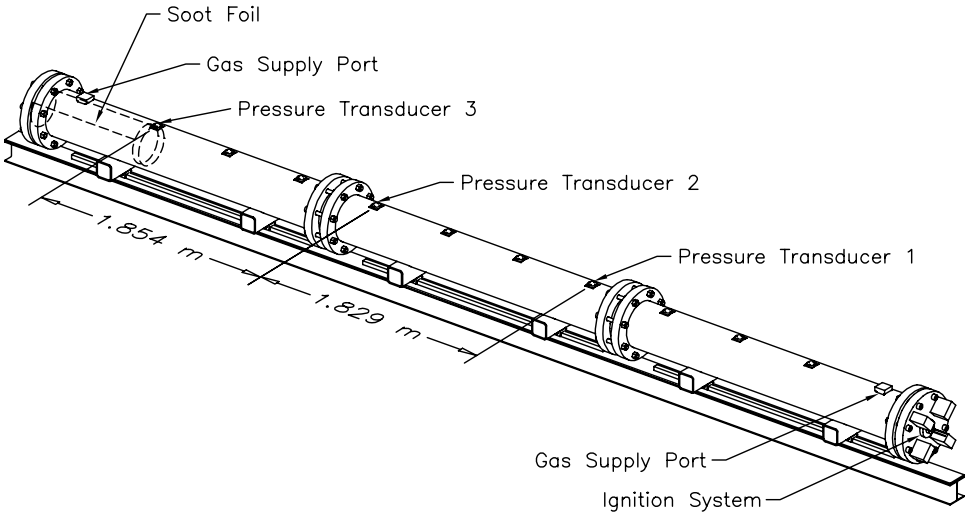

Figure 1: GALCIT 280 mm diameter gaseous detonation facility.

minimum tube diameter. The critical energy required to initiate a detonation is proportional to the cube of the cell width for a spherical source, and directly proportional to the cell width for a planar source (Lee et al. 1982), so fuels which produce smaller cell sizes are more sensitive to detonation. Although direct initiation is not considered feasible for PDE operation, cell width plays an important role in determining if detonations are possible in a given size device. For example, the smallest open area in a tube must be larger than one cell width for deflagration-to-detonation (DDT) to occur. This is an important issue in PDEs which use DDT initiators.

2 Facility Description

Detonation cell width experiments were performed in the gaseous detonation tube (GDT) (Akbar 1997, Akbar et al. 1997) shown in Fig.1.

The stainless steel detonation tube is 7.3 m long and has an internal diameter of 280 mm. Before each shot, an aluminum sheet or foil (0.61 m by 0.91 m by 0.5 mm) is rolled, riveted to a steel ring and covered in a light layer of soot. The foil is inserted into the downstream end of the tube and anchored in place. The entire tube is evacuated to about 10 Pa, and then filled by the method of partial pressures. Pressure in the tube is measured by an electronic Heise 901a gauge which is accurate to $\pm$ 0.17 kPa. Hexane

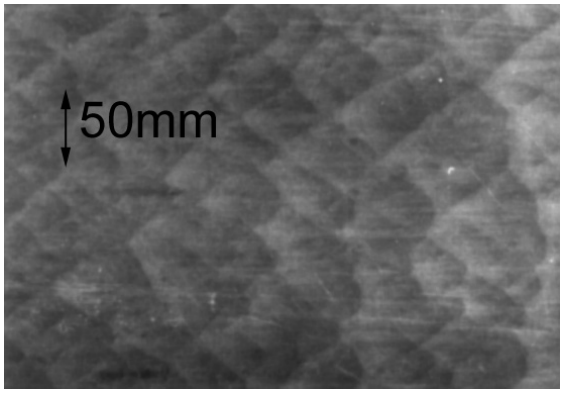

Figure 2: Soot foil for shot 1007: C_6H_{14}+9CO+14 Air. Detonation propagated right to left.

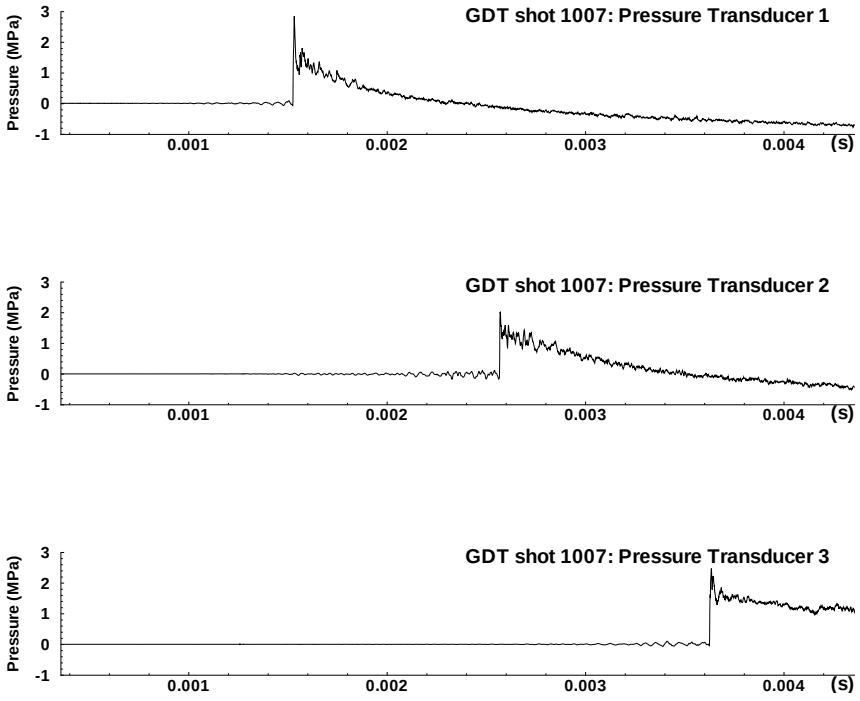

Figure 3: Pressure traces for shot 1007.

is injected into the evacuated tube through a septum. The partial pressure of hexane (vapor pressure of 20 kPa at 298 K) was low enough to ensure that the fuel had vaporized. The partial pressure recorded was at most 0.11 kPa higher than the value calculated based on the liquid volume injected, so this error was within the accuracy of the gauge.

The remaining gases are added to the tube by the method of partial pressures, and the mixture is circulated with a bellows pump for 5 minutes. Ignition is by an exploding wire, created by discharging a 2 μF capacitor charged to 9 kV, through a copper wire, initiating an oxy-acetylene driver which is injected just prior to ignition. The equivalent energy of the blast wave transmitted to the test gas is about 70 kJ. Experiments were limited to mixtures producing reflected pressures of 5 MPa, the design limit of the facilty. In cases where the reflected pressure of the mixture would exceed 5 MPa, the test was performed at the highest initial pressure possible, then the cell widths for 100 kPa initial pressure were estimated by assuming the cell width varies in inverse proportion to the initial pressure. These data are presented as 'extrapolated'. All experiments in the GDT were carried out at room temperature, nominally 295 K.

Three PCB pressure transducers, mounted along the tube, record the detonation pressure and time-of-arrival of the wave which is used to calculate a wave speed (Fig. 3). The chemical equilibrium program STANJAN (Reynolds 1986) is used to calculate the Chapman-Jouguet wave speed, pressure, and temperature. The wave speed obtained from the pressure transducers is checked against the calculated value and is typically within $\pm$ 1%. The shock triple points in the passing detonation scour a cellular pattern on the soot foil (Fig. 2). There can be quite a range of cell widths recorded for a particular mixture due to the inherent irregularity of the cells. About 10 measurements are made on each foil, and a minimum, a maximum, and an average cell width are recorded. The minimum and maximum give an indication of the range of cell sizes present on a foil. There are also variations in measurement from observer to observer. These can be on the order of $\pm$ 50% (Tieszen et al. 1991).

3 Cell Width Measurements

3.1 C_6H_{14} Mixtures with O_2-N_2

The sensitivity of stoichiometric C_6H_{14}-O_2 to nitrogen dilution was investigated. Since the reflected detonation pressure for these mixtures initially at 100 kPa exceeded the facility limit, experiments were performed at 40 kPa or at the highest initial pressure possible in the facility for each mixture. The cell width at an intial pressure of 100 kPa was estimated from these two data points. The average cell width is plotted against β in Fig. 4, where β is the ratio of N_2 to O_2 concentration in the mixture (β=3.76 for air). The minimum and maximum cell widths measured are indicated by the error bars. The cell width increased from 1.7 mm at $\beta = 0$ to 51.1 mm at $\beta = 3.76$. Extrapolated cell widths were a factor of 2 smaller than those previously measured at 100 kPa by Beeson et al. (1991).

Fuel	Cell width (mm)	Reference
H_2	10.9	CIT
CH_4	280	Moen et al. (1984)
C_2H_2	10	Knystautas et al. (1982)
C_2H_4	22.8	CIT
C_3H_8	51.3	CIT
C_6H_{14}	51.1	CIT

Table 1: Comparison of cell width measurements of various stoichiometric fuel-air mixtures at 100 kPa.

A comparison was made between the hexane and other fuels (Table 1). Cell widths obtained at different β values are shown in Fig. 6 for H_2, C_2H_2, and in Fig. 5 for C_2H_4, C_3H_8, and CH_4, all at 295 K and 100 kPa. 'CIT' refers to unpublished cell width measurements previously made in the GDT at GALCIT. Hexane cell widths appear to be similar to those of propane, C_3H_8. Cell widths for hexane are smaller than those for methane, and larger than those for acetylene or hydrogen. Tieszen et al. (1991) found little variation in cell width with increasing molecular weight for alkanes from ethane to decane, but found differences between hydrocarbons with differing degrees of bond saturation, with alkynes and alkenes producing a smaller cell width than alkanes.

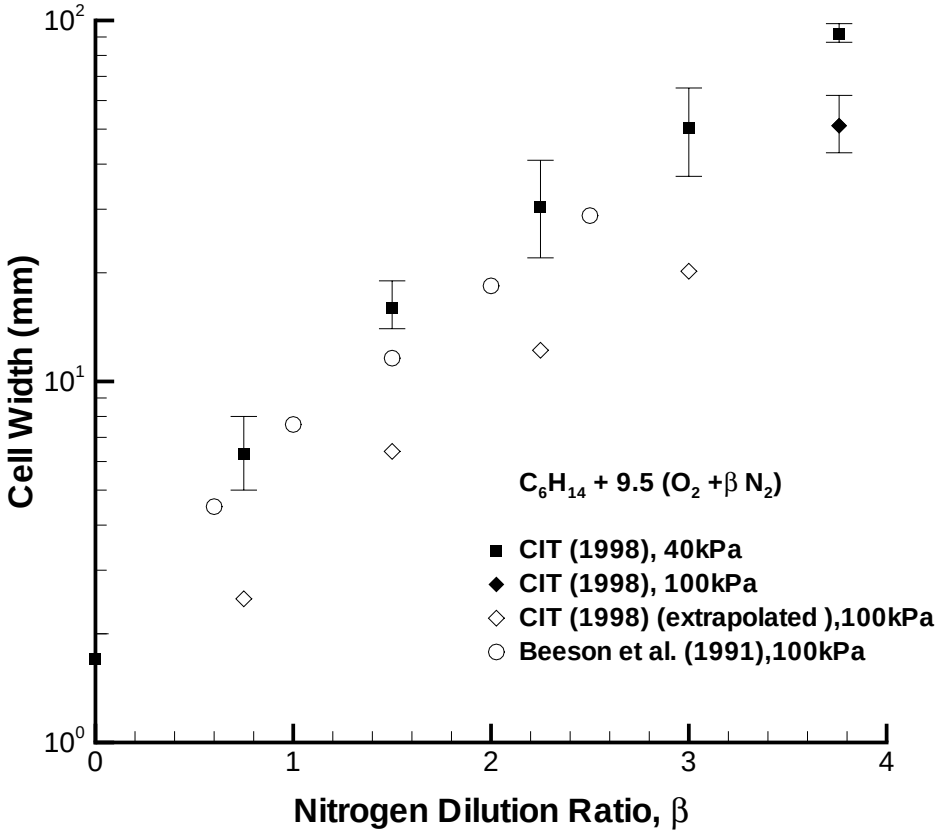

Figure 4: Cell width measurements for N_2 dilution of C_6H_{14}-O_2 mixtures. Experiment parameters are given in Table A

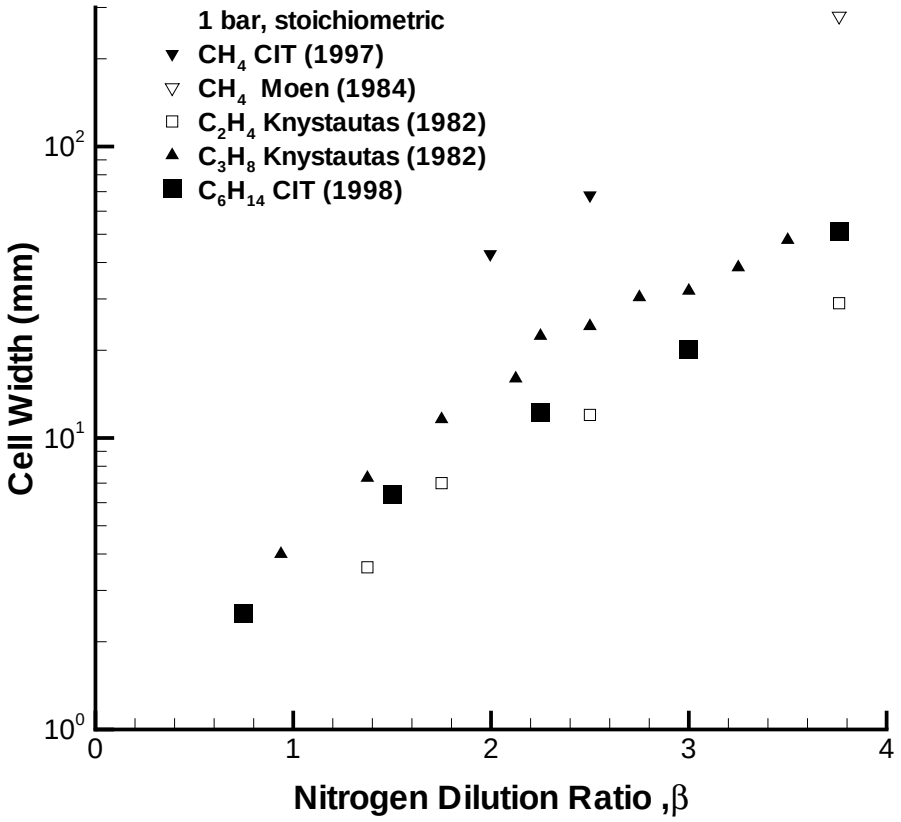

Figure 5: Comparison of cell width measurements for N_2 dilution of CH_4, C_2H_4, C_3H_8 and C_6H_{14}-O_2 mixtures. C_6H_{14} data is the same as that presented in Fig.4

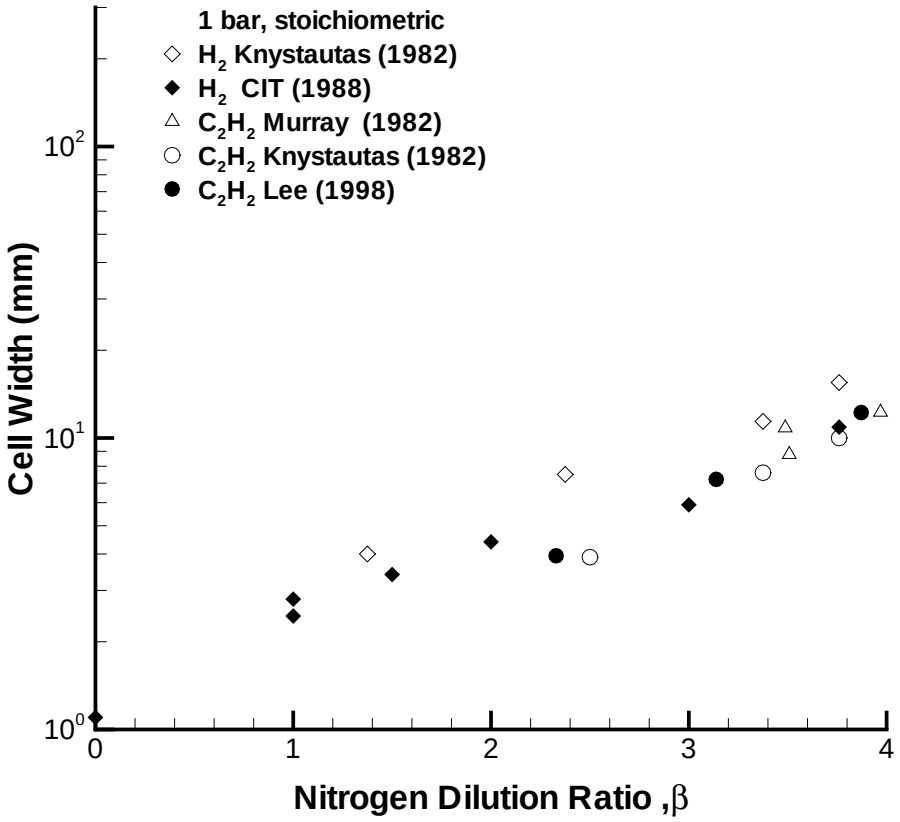

Figure 6: Comparison of cell width measurements for N_2 dilution of H_2, C_2H_2 mixtures with O_2.

3.2 Sensitization of C_6H_{14}-air

A series of investigations were made into the sensitizing effects of adding H_2, C_2H_2, C_2H_4 or CO to C_6H_{14} at 295 K and 100 kPa. The amount of sensitizer was calculated as a mass fraction in the sensitizer-hexane mixture. The appropriate amount of air was added to maintain a stoichiometric mixture. Results are shown in Figs. 7 to 10, with cell width plotted against the percentage (by fuel mass) of sensitizer in the fuel mixture. H_2, C_2H_2, and C_2H_4 mixtures show a gradual decrease in cell width as the fraction of fuel additive increases; H_2 and C_2H_2 are more effective than C_2H_4. There is no significant variation in cell width for mixtures containing 10 - 70% CO. In mixtures with CO fractions increasing beyond about 75% the cell width increases, indicating the CO acts as an inhibitor. This result is reasonable in view of the subsequent results which confirm the sensitivity of CO mixtures to the presence of hydrogenous species, since the measured cell width increases (indicating reduced sensitivity to detonation) when the initial fraction of H in the mixture is decreased.

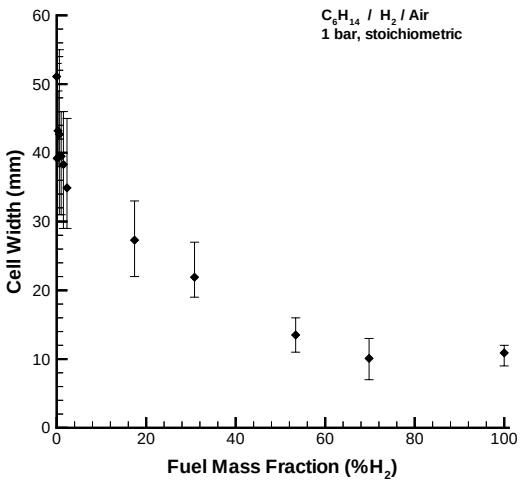

Figure 7: Cell width measurements for H_2 addition to C_6H_{14} in air. Experiment conditions are given in Table A.

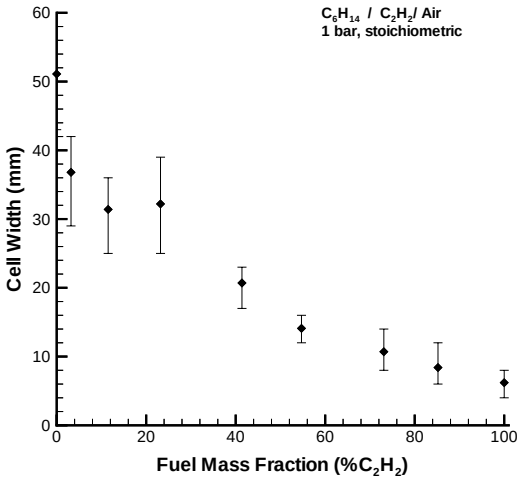

Figure 8: Cell width measurements for C_2H_2 addition to C_6H_{14} in air. Experiment conditions are given in Table A.

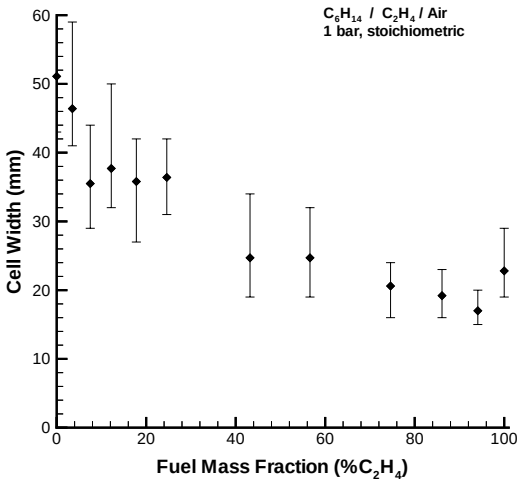

Figure 9: Cell width measurements for C_2H_4 addition to C_6H_{14} in air. Experiment conditions are given in Table A.

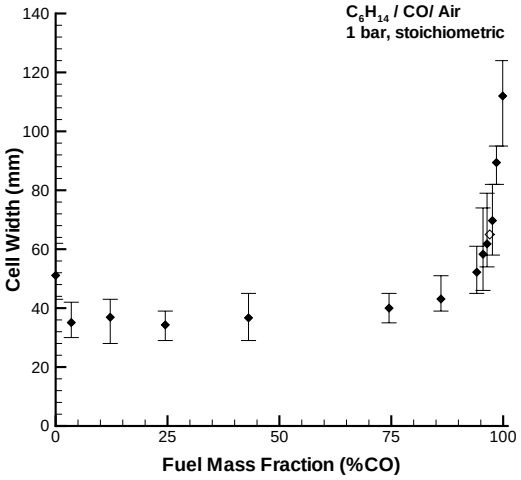

Figure 10: Cell width measurements for CO addition to C_6H_{14} in air. Experiment conditions are given in Table A.

3.3 Addition of H_2, C_2H_2, C_2H_4, and C_6H_{14} to CO-air

Carbon monoxide is of fundamental importance as a principal intermediate product of hydrocarbon combustion, however there are very little data available on the detonation characteristics of CO. The reaction mechanism is relatively simple and has been studied extensively (Gardiner 1984). In the presence of even trace amounts of hydrogen, the oxidation of CO takes place almost entirely by reaction (1) rather than by the spin-forbidden reaction (2).

$$CO + OH \rightarrow CO_2 + H \tag{1}$$

$$CO + O + M \rightarrow CO_2 + M \tag{2}$$

Early reseachers has found a dramatic increase in the reactivity of carbon monoxide with the addition of water vapor or other substances containing hydrogen (Dixon 1896, Kistiakowsky et al. 1952, White and Moore 1965). The hydroxyl radical promotes oxidation and drastically reduces the induction time Addition of only 0.02 % H_2 to a CO-air mixture results in a reduction in the calculated reaction zone thickness of three orders of magnitude.

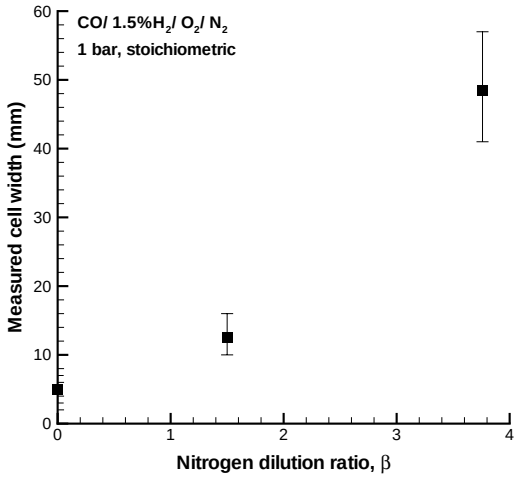

Figure 11: Cell width measurements for N_2 dilution of stoichiometric CO-5% H_2-O_2. See Table A for experiment conditions.

The addition of different hydrogenous species to CO-air mixtures was investigated. The fuels H_2, C_2H_2, C_2H_4, and C_6H_{14} were chosen so as to study the effects of varying atomic hydrogen content and chemical structure. Detonation pressure, velocity and cell width measurements were made. All mixtures were stoichiometric and at 100 kPa and 295 K initial pressure and temperature. Gases used were C.P. grade (99%) and no attempt was made to remove impurities. In these and all other experiments, 'air' was formed from 1 part O_2 with 3.76 parts N_2. This avoided using room air which might contain unknown quantities of moisture.

No detonation could be initiated in stoichiometric CO-O_2. The limiting fraction of H_2 that was necessary to detonate CO-air was found to be between 0 and 2 %(by fuel volume). Since the mixture CO-2% H_2-air resulted in highly irregular cells, a nitrogen dilution series was performed in the mixture CO-5% H_2 with stoichiometric O_2 (Fig. 11).

Cell width measurements were made for varying mixture volume fractions of H_2, C_2H_2, C_2H_4 and C_6H_{14} in CO-air (Fig. 12). In all cases, increasing the fraction of additive reduced the cell width. The rate of decrease of cell width is largest width fuel addition of H_2 and C_2H_2, followed by C_2H_4, then C_6H_{14}. This is consistent with results from Tieszen et al. (1991) who measured cell widths for hydrocarbon-air mixtures and found triply-bonded acetylene had smaller cell widths than doubly-bonded ethylene, which in turn had smaller cell widths than a straight-chain hydrocarbon such as hexane.

A detonation could be initiated in mixtures with only very small fractions of C_6H_{14} (down to 0.07 % of the total mixture). This was the lowest fraction attempted since we were limited by the accuracy of the gauge used during the filling process. In view of the sensitivity of CO oxidation to the presence of hydrogen, this was an interesting result. The hexane molecule contains many more H atoms than the other hydrocarbons considered and so hexane has the highest initial H atom concentration for a mixture at a particular additive concentration. Fig. 13 shows the measured cell width against the initial H atom concentration normalized by the initial CO concentration, where initial H atom concentration is defined as n times the fuel concentration for the fuel C_mH_n.

To investigate whether the hexane molecule is successful in releasing more H atoms to form OH radicals than an equivalent mixture fraction of the other additives, reaction zone parameters such as species concentrations and temperature were calculated using detailed chemical kinetics mechanisms. Chemical mechanisms were first validated by comparing induction times cal-

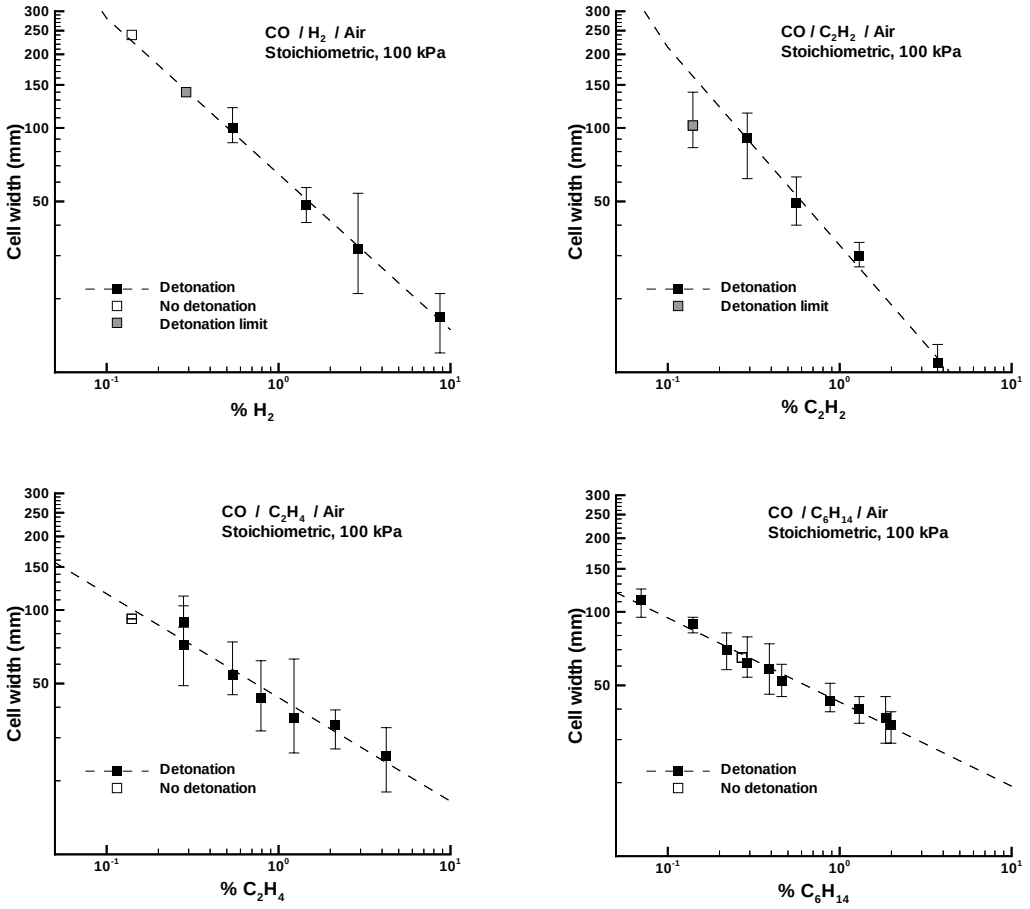

Figure 12: Cell width measurements for hydrogen or hydrocarbon addition to CO-air mixtures. Curves are interpolated from the cell widths of successful detonations. Error bars represent minimum and maximum measured cell widths. The detonation limit denotes a mixture where at least one failure was observed. About three experiments were performed for each mixture that resulted in a failure. Conditions and data are given in Table A

culated with a constant volume explosion assumption with measured shock tube induction times for the same mixtures. Mechanisms were validated against shock tube data for CO-H_2 mixtures and also for mixtures involving the hydrocarbon for which they were considered. The mechanism of War-

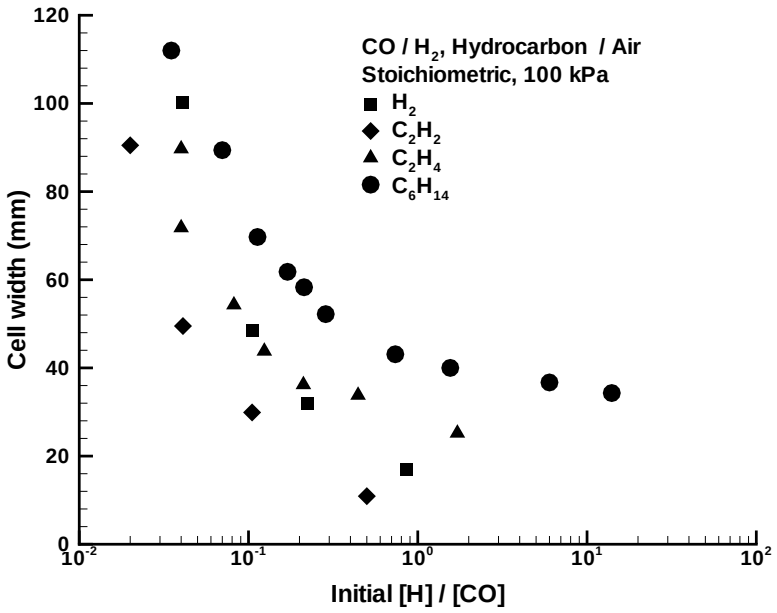

Figure 13: Measured cell width against initial H/CO ratio. Only successful detonations are shown.

natz and Karbach (1997) (34 species, 165 reactions) was chosen for mixtures containing H_2, C_2H_2 and C_2H_4. The mechanism of Curran et al. (1998) (550 species, 2500 reactions) was used for C_6H_{14} mixtures. Some validations are shown in Fig. 14 and 15. The mechanisms both perform very well against the CO-H_2-O_2 data of Dean et al. (1978). The largest discrepancy is for the Curran mechanism against the data of Burcat et al. (1996) for which the mechanism underpredicts the experimental results by a factor of 2. Davidson et al. (1999) compared ignition delay times calculated by the Curran mechanism with their shock tube data for heptane mixtures and found the same trends: the mechanism shows a similar temperature dependence as their data but the calculated ignition times are a factor of two shorter than the measured values. A discussion of the range of validity of detailed reaction mechanisms for detonation conditions, possible sources of error in shock tube induction time data and the applicability of a constant-volume calculation for the validation process is given in Schultz and Shepherd (2000).

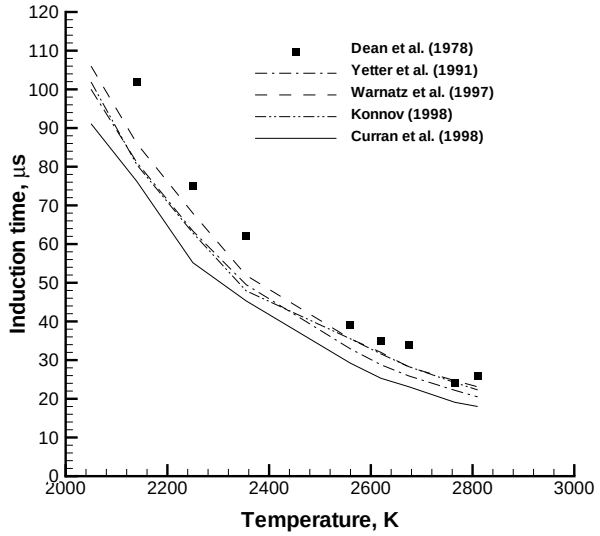

Figure 14: Mechanism validation for CO-H_2-O_2-Ar mixtures. Shock tube data is for the mixture 0.049% H_2, 1.01% O_2 , 3.28% CO, Ar.

A one dimensional Zel'dovich-von Neumann-Doring (ZND) code was used together with the validated mechanisms and CHEMKIN II (Kee et al. 1989) chemical kinetics subroutines to calculate the variation of temperature and species concentrations through the reaction zone. The reaction zone length is typically defined as the distance between the shock and the location of the maximum temperature gradient and can be related to the cell width by a constant of proportionality, A. This constant has been shown to be different for fuel-O_2 and fuel-air mixtures (Westbrook 1982) and also to vary with the equivalence ratio (Shepherd 1986). In spite of this, both reaction zone length and cell widths decrease with decreasing critical initiation energy and are a useful measure of the sensitivity of a mixture to detonation. Fig. 16 shows measured cell widths against reaction zone lengths. There are some significant deviations from the expected linear relationship. For instance, some of the acetylene mixtures have shorter reaction zone thicknesses due to an early 'bump' (and therefore change in curvature) in the temperature profile. Reaction zone lengths were redefined as the location of the peak in OH mole fraction. The correlation with measured cell width appears more

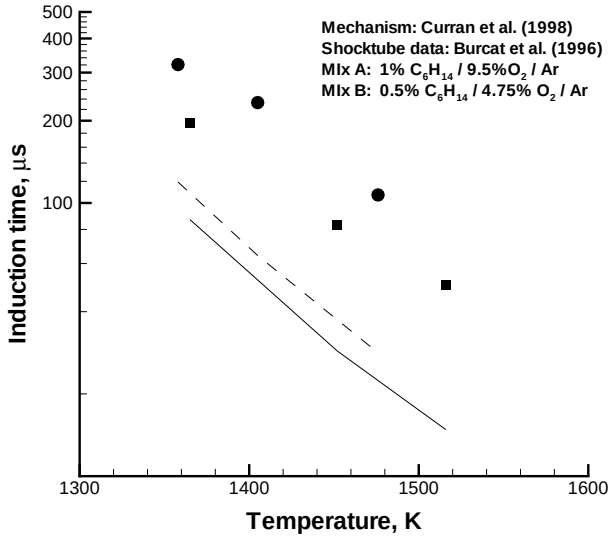

Figure 15: Mechanism validation for C_6H_{14}-O_2-Ar mixtures. Circles and dashed lines correspond to data and calculations respectively for mixture A. Squares and solid lines correspond to data and calculations respectively for mixture B.

linear (Fig. 16) and this definition of reaction zone thickness will be used for the rest of this section. Values between 25 and 35 were obtained for A.

To track the production of the OH radical, species concentrations of CO, CO_2, OH, O, H and CH were calculated through the reaction zone. As an example, some species concentrations for mixtures with 2% and 30% H_2 (by fuel fraction) are shown in Fig. 17. A large difference in the amount of OH produced by the two mixtures can be seen. The calculated peak OH concentration is shown in Fig. 18 against initial [H]/[CO] ratio. For small initial [H]/[CO] ratio, all mixtures produce about the same peak OH mole fraction. With the addition of more significant fractions of hydrogen or hydrocarbon, the calculated peak OH mole fraction is highest for H_2, C_2H_2 and C_2H_4. C_6H_{14} produced the smallest peak mole fraction for a given initial [H]/[CO] ratio. A closer look at the species profiles for these C_6H_{14} mixtures shows a peak in the CH and CO mole fraction profiles (Fig. 19). The fall-off in OH production might be attributed to competition between OH and CH

formation reactions.

As discussed above, the cell width can be related to the reaction zone thickness by a constant of proportionality, A. The reaction zone thickness is transformed to an induction time by dividing by the particle post-shock velocity. The induction time, τ, may be modeled by identifying a dominant overall reaction for the mixture. A simplified expression for the induction time for a reaction rate with a simple Arrhenius dependance is shown in (3).

$$\tau = \frac{K}{[OH][CO]} \exp \frac{E_A}{RT_s} \tag{3}$$

where T_s is the post-shock temperature. As the fraction of hydrogen or hydrocarbon added was small, thermal differences between the mixtures considered are small and T_s is approximately constant, so the temperature term plays a negligable role for these mixtures. Correlating the measured cell width against the inverse of the product of the OH and CO concentrations results in a linear relationship for hydrogen and all the hydrocarbons considered (Fig. 20). The species mole fractions are evaluated at the OH peak. Data for H_2, C_2H_4 and C_6H_{14} collapses onto a single curve while the C_2H_2 mixtures obey the similar linear relationship but the data fall a factor of two below that of the other additives. This relationship between the cell size and the OH and CO concentrations suggests that reaction (1) is in fact a dominant reaction for CO mixtures in the presence of hydrogenous species.

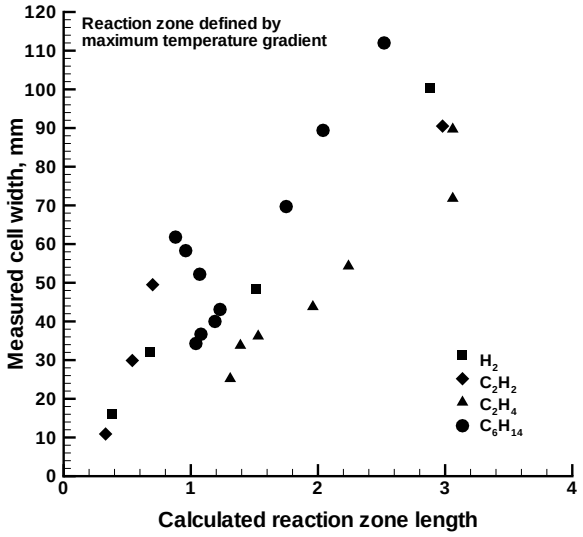

a)

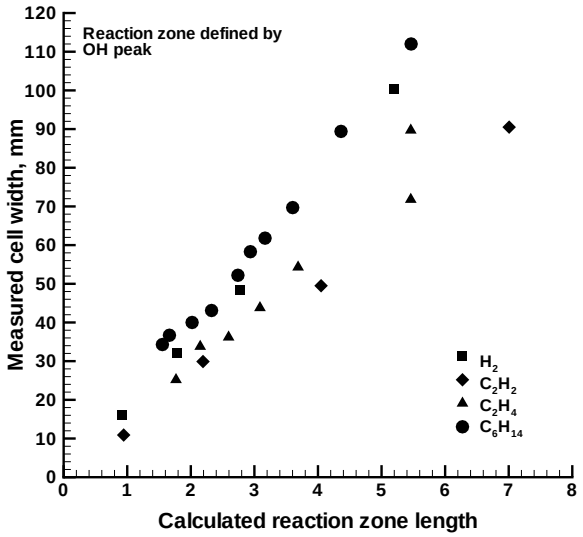

b)

Figure 16: Cell width measurements versus reaction zone thickness in CO-O_2 mixtures with hydrogenous additive at 100 kPa. The reaction zone thickness is defined by a) the location of the maximum temperature gradient or b) by the location of the OH peak.

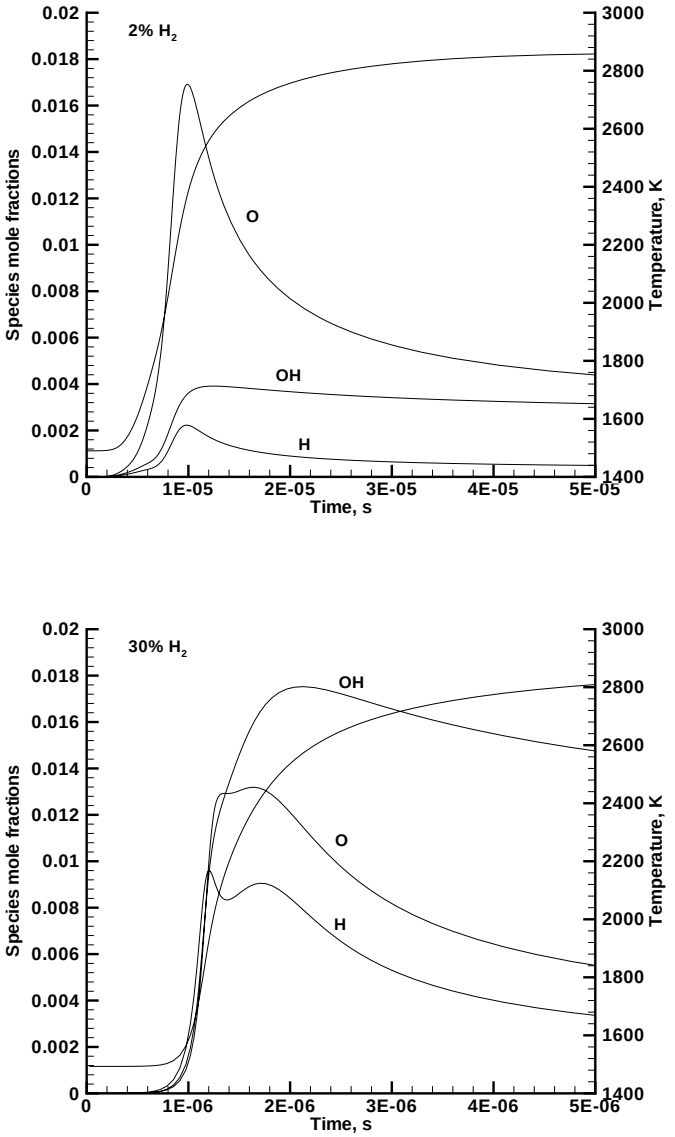

Figure 17: Calculated species mole fractions through the reaction zone in stoichiometric CO-H_2-air mixtures. H_2 quantities are by fuel mole fraction.

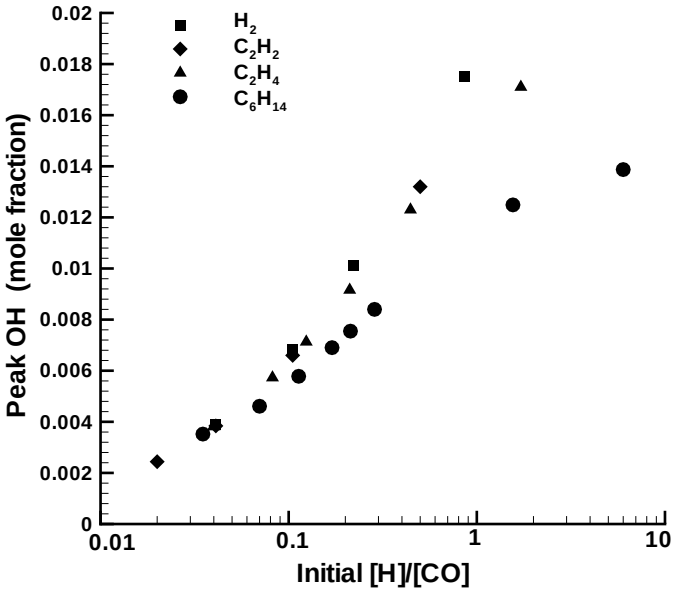

Figure 18: Peak OH mole fraction against initial [H]/[CO] ratio.

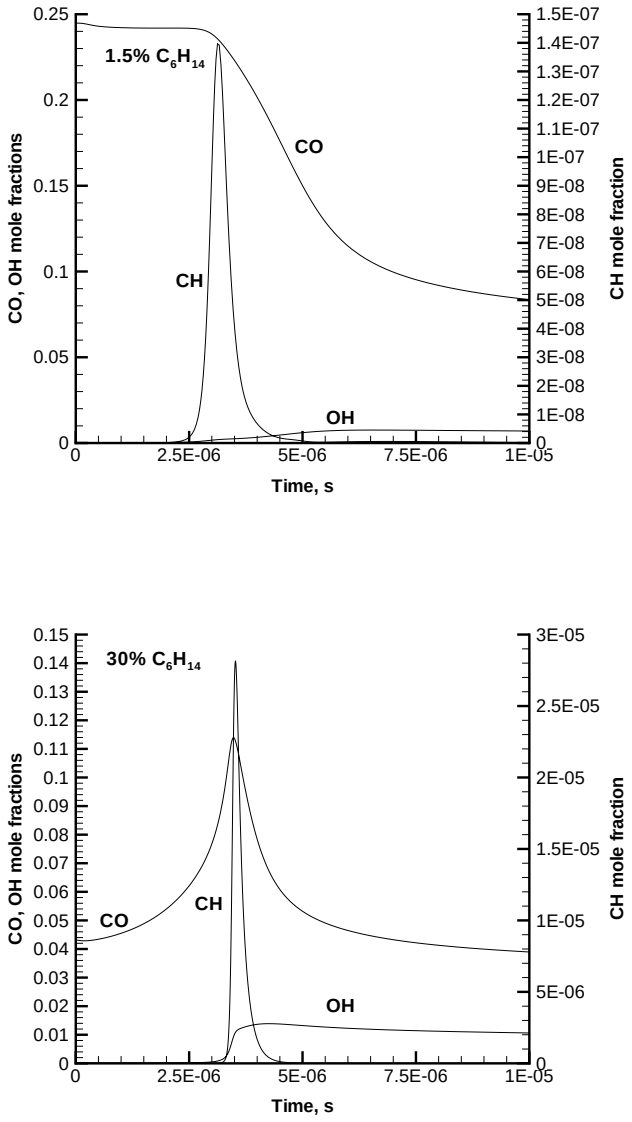

Figure 19: Calculated species mole fractions through the reaction zone in stoichiometric CO-C_6H_{14}-air. Note the differences in scale on the ordinate axis.

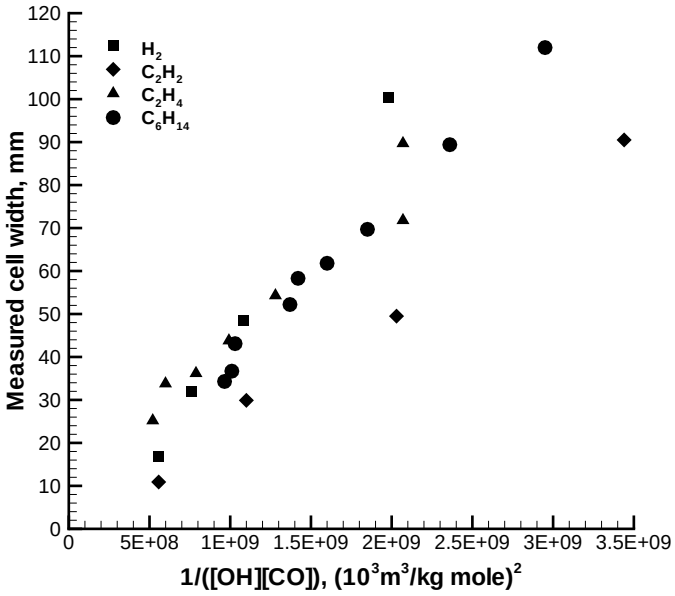

Figure 20: Correlation of measured cell width against the parameter 1/([OH][CO]). Species concentrations are calculated by a ZND code and evaluated at the OH peak.

3.4 Decomposed JP-10 Surrogate (HCS)

Brabbs and Merritt (1993) investigated the fuel-rich catalytic combustion of JP-10 for a range of equivalence ratios. We have used their results to create a mixture similar to the decomposition products and tested this mixture in our detonation tube. The mixture chosen for this study (Table 2) resulted from JP-10 combustion at an equivalence ratio of 5.06, with a reaction temperature of 1220 K . Group 2 hydrocarbons are those with 3 or more carbon atoms. The remaining fraction consisted of condensible products which were not analyzed.

CO_2	H_2	CO	CH_4	C_2H_2	C_2H_4	Group 2	O_2	N_2
3.37	8.07	14.70	2.88	0.73	4.24	3.03	1.38	60.79

Table 2: JP-10 catalytic combustion products

A hydrocarbon surrogate (HCS) blend was made by omitting the O_2, N_2 and CO_2 from the mixture given in Table 2. Hexane was chosen as a representative larger hydrocarbon from Group 2. Four of the compoents of the blend (H_2, CO, CH_4, and C_2H_4) were premixed by the manufacturer to an accuracy of ± 2 % on each component. This was done to improve the repeatability of the tests.

The HCS blend was mixed with a stoichiometric amount of O_2 and diluted with N_2 (Table 7). Experiments were performed at 295 K and at the maximum pressure possible in the facility. The pressure was limited by the design strength of the tube. Cell widths were obtained for several β values (Fig. 21), and decrease from 27.6 mm for $\beta = 3.76$ (i.e. fuel blend-air) to 1.0 mm for $\beta = 0$ (i.e. fuel blend-oxygen), a decrease in the spherical critical initiation energy of four orders of magnitude.

The mixture for shot 1067 is the HCS blend together with the O_2 and N_2 remaining after the catalytic combustion. Sufficent air was added so that the mixture was stoichiometric. Since most of the original oxygen had been consumed in the combustion of JP-10, this resulted in a β ratio greater than that of air. The cell width for this case was 55.8 mm which is very close to the 51.1 mm cell width measured for C_6H_{14}-air (Section 3.1). If the HCS blend is mixed with stoichiometric O_2 and no N_2 is added beyond that which would result from the catalytic combustion, $\beta = 1$ and the extrapolated cell width at 100 kPa is about 4 mm. Thus we estimate the spherical critical

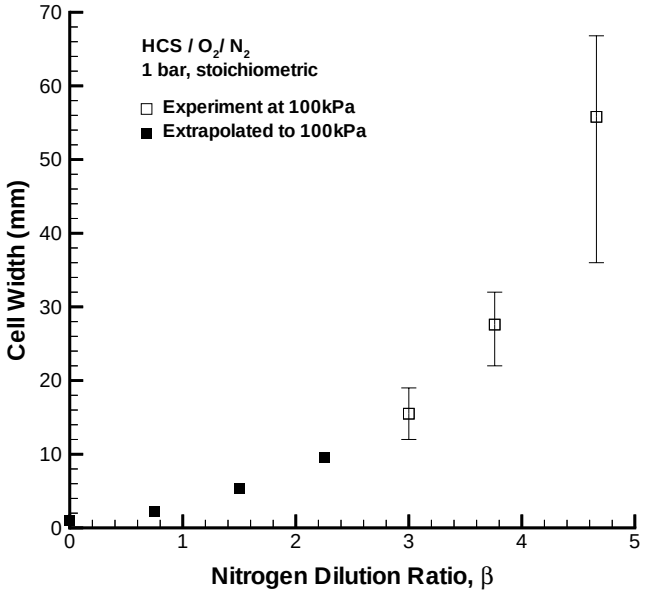

Figure 21: Cell width measurements for N_2 dilution of a hydrocarbon blend representative of decomposed JP-10. The initial pressure was increased with increasing N_2 dilution.

initiation energy can be reduced by three orders of magnitude if the combustion products of JP-10 catalytic combustion are detonated in oxygen rather than in air.

Part II
Homogeneous and Heterogeneous Detonations in C_6H_{14} and $C_{12}H_{26}$

4 Introduction

Liquid hydrocarbon fuels can be pre-heated to vapor phase, or alternatively, injected into a combustion chamber in a fine spray. Papavassiliou et al. (1992) initiated detonations in decane sprays of 5μm and found the cell size increased by a factor of two over cell sizes obtained for vapor phase detonations at 100 °C. They report a cell width of 4 mm for decane spray-oxygen detonations at an equivalence ratio of about 0.95.

In this study, a jet-initiation facility was used to try to detonate both vapor phase and droplet phase mixtures of a representative heavy hydrocarbon (dodecane). Cell width measurements are not available for dodecane, so the critical nitrogen dilution limit was used as a measure of the detonability. Vapor phase dodecane experiments were performed at 380 K. Detonations were initated in vapor phase hexane mixtures for comparison.

5 Facility Description

Experiments were performed in the HYJET facility (Fig. 22). A brief facility description is given below, for more details see Krok (1997). The facility consists of two vessels, a driver and a receiver chamber, initially separated by a Mylar diaphragm. The driver has a volume of 0.028 m^3 and an inner diameter of about 114 mm, although there are variations in cross-sectional area along its length. Interchangeable nozzles mate to the end of the driver and retain the diaphragm. Only the 92 mm diameter nozzle was used in these experiments. The driver extends into the receiver, which has a volume of 1.19 m^3 and an outer diameter of 0.91 m.

The receiver can be heated to a maximum gas temperature of 383 K and was maintained at 380 K for the vapor-phase dodecane experiments. The

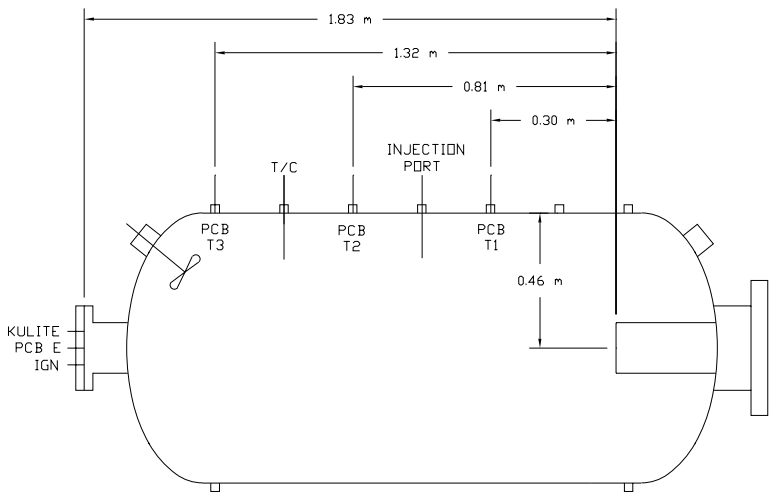

Figure 22: HYJET receiver instrumentation. (Driver vessel not shown.)

vessel walls are heated by condensing steam inside the vessel and by electrical heating pads and tapes. The temperature is monitered by a thermocouple gauge positioned in the receiver vessel.

Both vessels are evacuated to less than 40 Pa, then filled by the method of partial pressures. The liquid fuel is injected through a septum. Sufficient fuel was injected to achieve the required partial pressure; the volume of hexane injected varied between 1 and 1.3 times the calculated volume and the dodecane required 1.1 and 1.6 times the calculated amount. There was no obvious correlation between the volume required and the other test parameters (see Appendix A). A similar effect was observed by Tieszen et al. (1991) when vaporizing liquid hydrocarbon fuels up to decane. The amount of liquid fuel required was 1.25 - 2 times the amount calculated, with the error increasing as the molecular weight of the fuel was increased. It was determined the soot in the facility absorbed fuel from the gas phase. It is expected that a similar effect occurs in the HYJET facility.

The driver mixture is initiated by a 30 kV spark. More detailed driver characteristics are given below. A thermocouple and three PCB transducers (T1,T2,T3) are located along the receiver and a fourth PCB is located on the end flange as shown in Fig. 2.1. These PCB transducers record the pressure

and time-of-arrival of the detonation wave. The trigger for the driver spark also triggers the data acquisition. The driver flange is instrumented with two pressure gauges (a PCB and a Kulite) and thermocouple gauge.

6 Driver Characterization

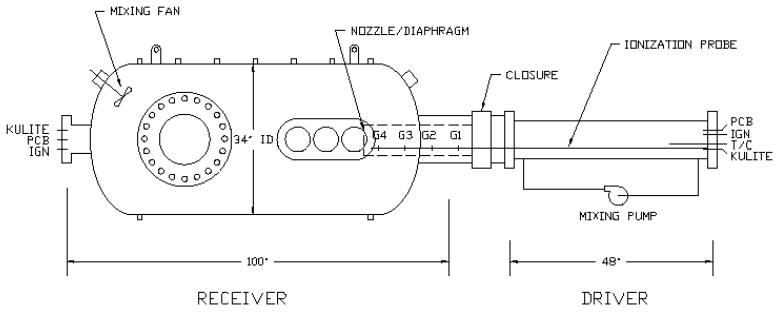

Figure 23: Ionization gauge located in the driver of the HYJET facility. The receiver contained air at 1 atm.

The driver mixture was 60% H_2, 15% O_2, 25% N_2 at an initial pressure of 1.114 bar. The same driver was used throughout this series of experiments. Various H_2, O_2, N_2 driver compositions had been previously investigated (Krok 1997), by determining the lean limit of detonation initiation in the receiver. For receiver mixtures that were 0-30% H_2 in air at 1 atm, it was determined that the above driver was most effective, as it was able to give prompt initiation with only 24% H_2 in the receiver mixture, a D/λ ratio of 4.3, where D is the diameter of the jet and λ is the detonation cell size of the mixture. A driver with no N_2 dilution required the receiver mixture to contain more than 26% H_2 before it could be detonated.

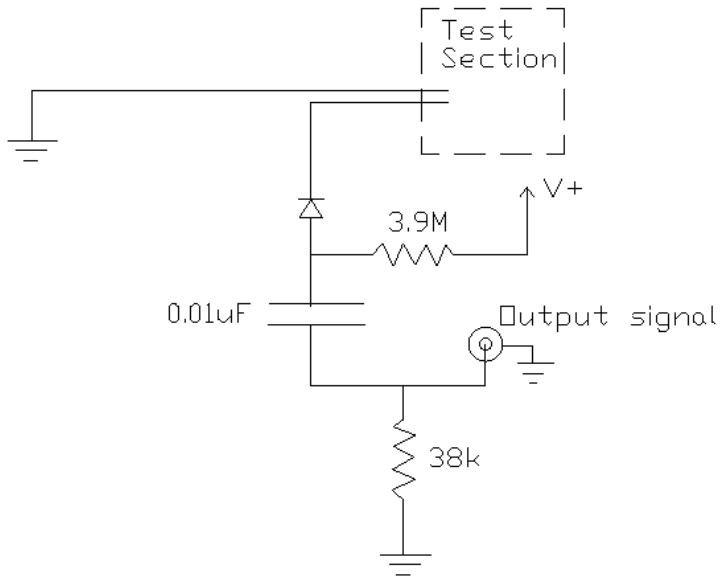

Figure 24: Schematic of the ionization gauge circuit, V^+=12V.

Krok's results indicated the 60% H_2, 15% O_2, 25% N_2 driver may be transitioning to detonation, but there wasn't sufficient instrumentation in the facility to be sure. To characterize the driver more thoroughly, an ionization probe has been built consisting of four gauges (G1, G2, G3, G4) mounted on a sting extending from the back flange of the driver (Fig. 23). The gauges are 178 mm apart and G4 is positioned 100 mm upstream of the diaphragm location. The gauges are all positioned in the part of the driver that is of uniform cross-sectional area. A schematic of the ionization gauge circuit is shown in Fig. 24. Time-of-arrival data and wave speeds (Fig. 25) show that the driver does indeed transition to detonation, and at 100 mm from the diaphragm it is probably an overdriven detonation as the CJ velocity of the driver mixture is calculated to be 2571 m/s. The receiver mixture was air at 1 atm.

A subsequent study (Pfahl and Shepherd 1999) determined the critical N_2 dilution limit for H_2-O_2 mixtures in the receiver of the same facility using a driver that didn't transition to detonation before the nozzle exit. Pfahl and Shepherd (1999) found $8 \leq D/\lambda \leq 11$ which, as expected, is higher than the ratio of around 4 determined for the detonating driver. Results for other flame-jet drivers also show higher D/λ ratios: Carnasciali et al. (1991)

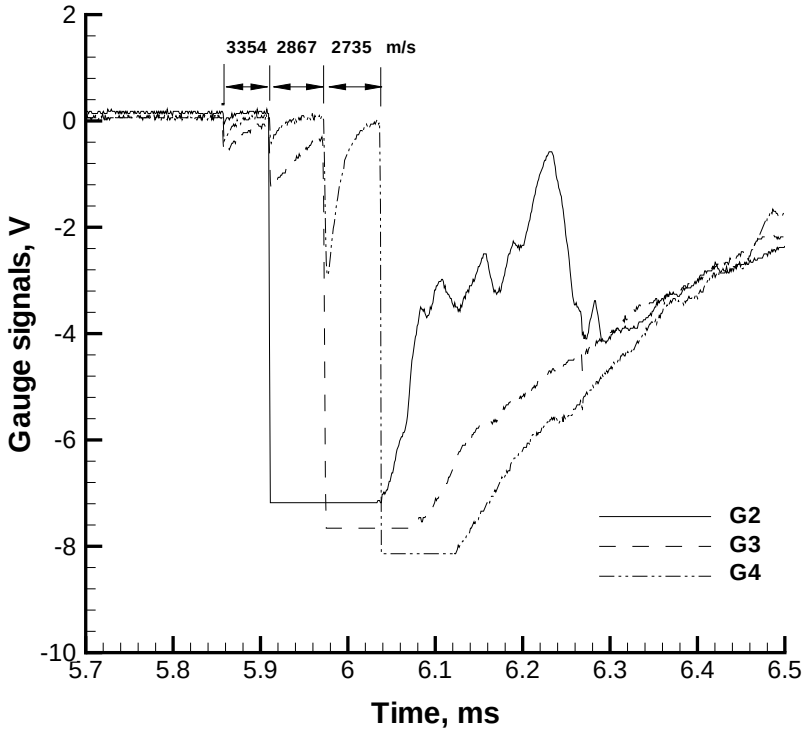

Figure 25: Time-of-arrival data from ionization gauges in the driver.

obtained $8 \leq D/\lambda \leq 15$, Bezmelnitsin et al. (1997) obtained $18.5 \leq D/\lambda \leq 24$.

The initial pressure for N_2-diluted drivers had been increased over 1 atm in an attempt to compensate for the reduced peak driver pressure. However, the peak pressures recorded in the driver were found to be higher than expected (Krok 1997). This was attributed to a dynamic effect of the confinement geometry, which is not considered by the equilibrium code used to predict the P_{AICC} pressure.

7 Vapor Phase Experiments in Hexane and Dodecane

7.1 Hexane

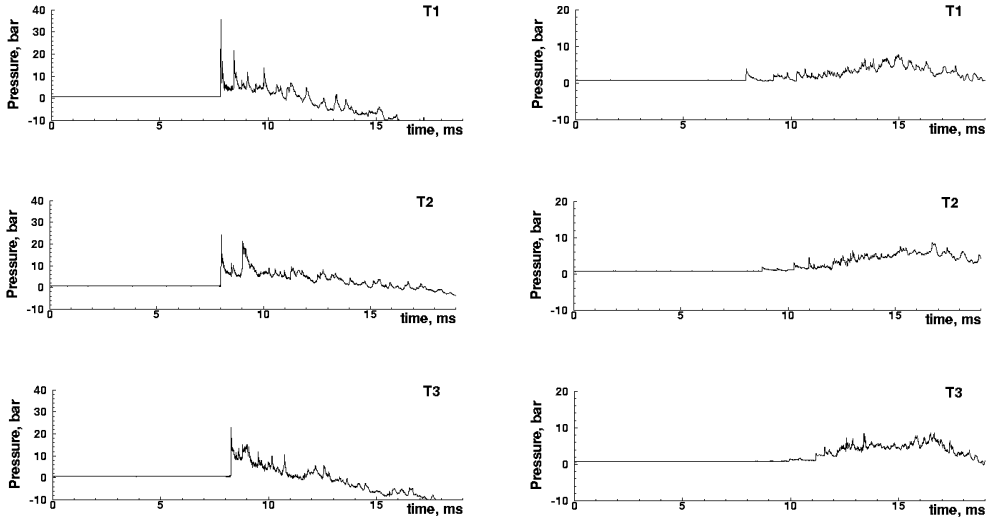

Figure 26: Pressure traces recorded along the receiver vessel wall for vapor phase C_6H_{14}-O_2-N_2 mixtures. On the left, $\beta = 2.25$ (shot 569). The initial pressure was 690 mbar, the initial temperature 298 K. On the right, $\beta = 3.0$ (shot 571). The initial pressure was 844 mbar, the initial temperature 296 K. Note the difference in scale on the ordinate axes.

The critical nitrogen dilution limit, defined as the maximum value of β

for a mixture that can still be detonated in this facility, was determined for stoichiometric mixtures of C_6H_{14}-O_2. To keep within the maximum design pressure of the facility, the partial pressures of C_6H_{14} and O_2 were kept constant for each shot. The total pressure then depended on the amount of nitrogen added. A detailed description of the conditions for each test is given in Appendix A. The vapor pressure of C_6H_{14} is high enough that the facility did not need to be heated for this series. Pressure traces are shown in Fig. 26 for two values of β, where β is the ratio of nitrogen to oxygen concentration in the mixture.

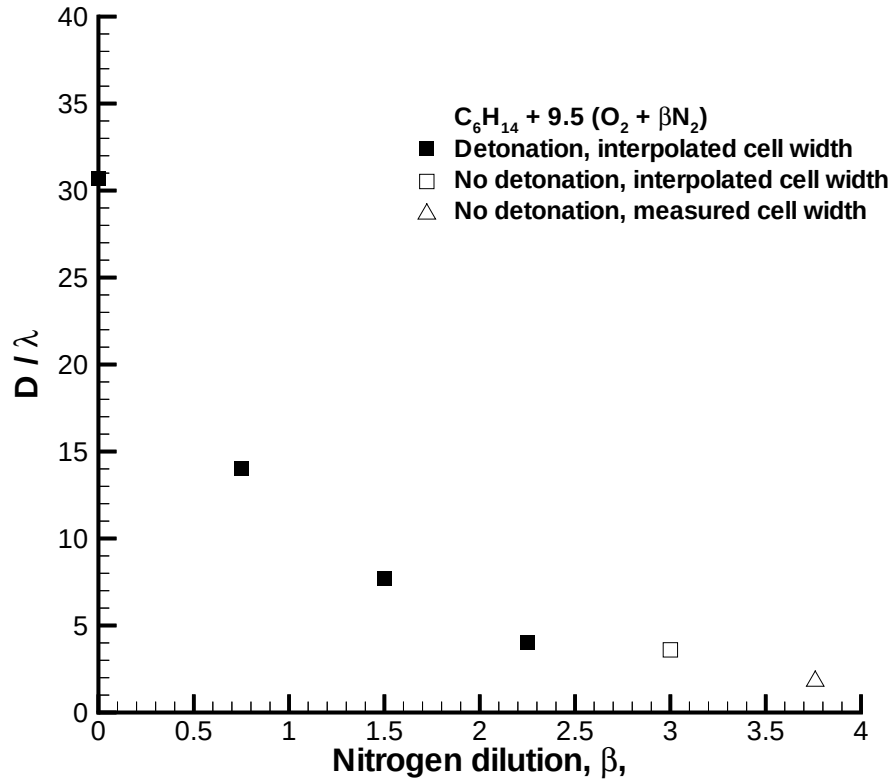

Figure 27: D/λ (nozzle diameter/measured cell width) variation with nitrogen dilution. Initial pressure increased with increaing N_2 dilution.

The equilibrium code STANJAN (Reynolds 1986) was used to calculate

CJ pressure, reflected pressure, and CJ velocity for each test. These calculated values, together with measurements, are given in Appendix A. Direct initiation was observed up to $\beta = 2.5$. For these cases, the peak pressure at the first transducer location (T1) is usually comparable to the calculated reflected wave pressure (around $2.5P_{CJ}$). The pressure decays as the wave passes from T1 to T3, but remains above P_{CJ}. The wave speed, obtained from the time of arrival at the three locations (T1,T2,T3), is up to 37% higher than the calculated CJ value, and decreases as the wave propagates from T1 to T3. Although the variation in the volume of liquid fuel injected was not systematic, the CJ wave speed corresponding to a mixture with the actual volume of fuel injected was also calculated and found to be about 5% higher than the stoichiometric value, so the excess liquid fuel injected (which is presumed to have been absorbed by the soot in the vessel) can not account for the high wave speed observed in experiments.

If the detonation in the receiver mixture is initiated near the jet exit, it will expand like an unconfined spherical detonation. The detonation wave will be curved rather than planar and will not propagate parallel to the wall but at an oblique angle. When the wave reaches T1 it may still have significant curvature so that the pressure recorded is close to the reflected pressure. The wave will flatten out as it propagates down the vessel decreasing the angle of incidence between the wave and the wall. For angle of incidence greater than about 60°, a Mach reflection will occur. This will affect the interpretation of the pressure measurements. It is also possible that the reactants are driven downstream by the jet flow and the detonation is initiated only after sufficient time for entrainment and an ignition delay period (see (Krok 1997)). In this case, the time-of-arrival at the three pressure transducers would be similar and a high wave speed would be inferred.

No detonation was directly initiated at $\beta \geq 3.0$ (Fig.26) although a delayed secondary explosion was observed. The peak pressures following the shock (0.4-0.2 MPa) and the wave speeds (around 500 m/s) were substantially less than the CJ values (P_{CJ}=1.72 MPa, U_{CJ} 1853 m/s). Cell width measurements made in the GDT facility for hexane were interpolated to match the pressure of the HYJET data (Appendix A). The critical D/λ ratio is about 4 (Fig. 27) and compares well with a previously determined value of 4.3 for this driver .

7.2 Dodecane

A similar nitrogen dilution series was performed in stoichiometric $C_{12}H_{26}$-O_2. Again, the partial pressures of $C_{12}H_{26}$ and O_2 were kept constant to keep the reflected pressure within facility design strength limits. The facility was heated to maintain a gas temperature of about 380 K, although variations of $\pm$ 1 degree did occur during the filling process. Measured and calculated properties for each test are given in Appendix A. A detonation could be directly initiated up to β=2.5 (Fig. 28). Both the wave speed and peak pressure were higher than the calculated CJ condition, but decayed as the wave propagated in the receiver. No detonation was directly initiated at β = 3.0 resulting in a critical N_2 dilution limit similar to hexane. No DDT regime was observed although a secondary explosion was observed in β = 3.0 mixtures after sufficient time had passed for shock reflection and shock focussing to precondition the mixture.

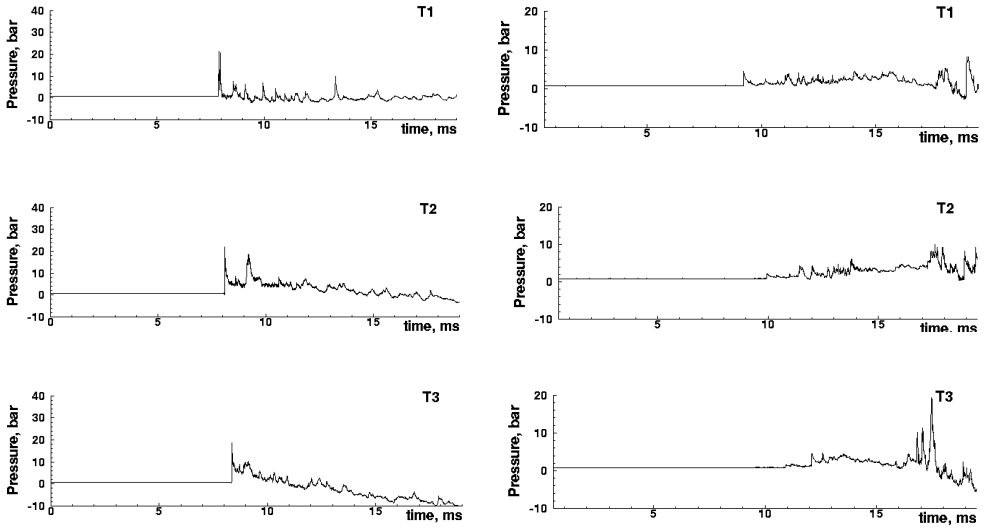

Figure 28: Pressure traces recorded along the receiver vessel wall for vapor phase $C_{12}H_{26}$-O_2-N_2 mixtures. On the left, β = 2.5 (shot 581). The initial pressure was 738 mbar, the initial temperature 381 K. On the right, β = 3.0 (shot 579). The initial pressure was 842 mbar, the initial temperature 380 K. Note the difference in scale on the ordinate axes.

No cell size data is currently available for dodecane. (Tieszen et al. 1991) measured cell widths for several hydrocarbons from hexane to decane and found little change in the cell width with increasing molecular weight (at 373 K, 100 kPa hexane-air had a cell width of 55mm, decane-air a cell width of 40mm). The study also determined there was little variation in cell size with temperature (297-373 K) for smaller hydrocarbons such as ethylene and propane. This is consistent with the present results since the critical β range for both hexane and dodecane was found to be the same. If D/λ ratio for jet-initiation is taken as a constant for a particular driver, the cell widths for the two fuels should be similar.

The critical nitrogen dilution limit was found to be repeatable for both C_6H_{14} and $C_{12}H_{26}$, in spite of differences in the volume of liquid fuel injected, which varied by as much as 20% (Appendix A).

8 Heterogeneous Experiments in Dodecane

8.1 Facility Modifications

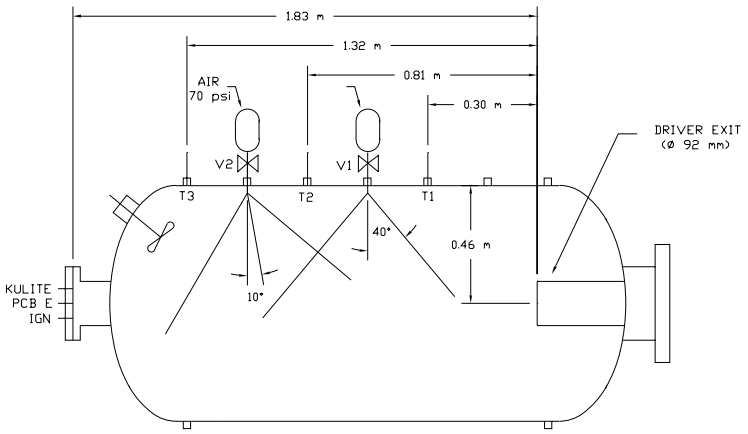

Figure 29: HYJET facility receiver vessel: two-port injection system configuration. (Driver vessel not shown.)

The HYJET facility (Fig. 29) was modified to allow liquid fuel injection. Two injection systems were tried and are described below. The initial mixture composition, pressure, and volume of liquid fuel in the receiver were to be the same as for the vapor phase experiments. The only mixture considered was stoichiometric dodecane-oxygen: 92 ml of liquid dodecane was injected into O_2 at 20.8 kPa. The mixing fan was run during the injection process, both to improve the homogeneity of the mixture and to assist in keeping the droplets suspended, but was turned off for the experiment. The driver was initiated immediately (about 0.5 to 1 s) after all the fuel had been injected to try to maximize the amount of fuel that remained suspended. Three PCB transducers (T1,T2,T3 in Fig. 22) located in the receiver vessel wall, together with a fourth transducer in the end wall, measure wave pressure. The time of arrival at the transducers T1-T3 is used to calculate the wave speed. The temperature was now only measured by gauges located on the external walls of the receiver vessel.

The nozzles used were obtained from McMaster-Carr (part# 3178KM3). The nozzle spray parameters were known for water and estimated for dodecane. The injection systems were tested with water outside the vessel, but the actual fuel injection could only be performed inside the vessel.

The nozzles produce a solid cone spray pattern with a theoretical half angle of 40° for water at 100 psi into the atmosphere. The spray angle increases when the surface tension of the liquid is reduced, and so is greater for dodecane (surface tension 24.98 mN/m at 25°C) than for water (surface tension 71.99 mN/m at 25°C). The spray angle is also likely to increase due the reduced pressure in the receiver. It should be noted that the theoretical spray angle is only useful in the immediate vicinity of the nozzle as the actual dimensions of the spray will be modified by gravity and moving gases.

The flow rate through the nozzles (3.0 ml/s at 70 psi) was used to determine when all the fuel had been injected. The flow rate, Q, was calculated by correcting the manufacturer measured flow rate for water at 70 psi for the specific gravity of dodecane. Specific gravity, SG, is the fluid property considered to have the most important effect on the flow rate. A simple check of the manufacturer's value was performed outside the vessel by injecting a measured volume of water through the nozzles and measuring the injection time required.

$$Q_{C_{12}H_{26}} = Q_{H_2O}\sqrt{SG_{H_2O}/SG_{C_{12}H_{26}}}$$

The nozzles are calibrated by the manufacturer to produces water droplets of 35 μm. Droplet size is affected by surface tension and by viscosity. The surface tension of dodecane is about 3 times less than that of water, which would reduce the droplet size, while the viscosity of dodecane (1.38 mPa s) is a factor of 1.5 times greater than that of water, which would increase the size of the droplets. The actual mixture distribution may also be affected by the droplets coalescing, by particles adhering to the vessel walls or by inhomogeneous particle distribution.

8.2 Results

Two liquid fuel injection systems were tried. In the first system, fuel was injected through the two ports shown in Fig. 29. Half the total volume of fuel was poured into each reservoir, then a 70 psi air supply forced the fuel to spray through the nozzles into the receiver vessel while the valves V1 and V2 were open. The valves were opened for time required for all the liquid to be injected, then the experiment was initiated as soon as possible (0.5-1 s) after the valves were closed. The pressure traces from this experiment (Fig. 30) clearly show only the decaying shock resulting from the driver detonation unsuccessfully diffracting into the receiver vessel.

This test was repeated with the vessel at an initial temperature of 65°C. Again the experiment was initiated as soon as the injection was complete. At this temperature, up to 45% of the fuel could vaporize if given sufficient time to reach equilibrium. The aim of increasing the initial temperature was twofold. It was hoped the fuel would partially vaporize so that a droplet might be surrounded by a fuel-oxygen vapor which would help sustain a detonation. In the process, the droplet size would be reduced, allowing the fuel to remain suspended for a longer time. The traces (Fig. 30) show a detonation was initiated, but only on reflection from the end wall of the vessel. The velocity of the reflected wave was 2070 m/s (U_{CJ} = 2259 m/s, P_{CJ} = 0.67 MPa). Heterogeneous detonation velocities have been observed to be 2-35% below the CJ value (Dabora et al. 1969).

The injection system was then redesigned in an attempt to decrease the injection time and reduce the amount of fuel lost to the vessels walls. A manifold with five nozzles was suspended from the top of the vessel (Fig. 31). This arrangement was to provide a more uniform injection, and in particular to improve the distribution around the driver exit. A reservoir of fuel was located above V2. Unlike the previous system, the reservoir held more fuel

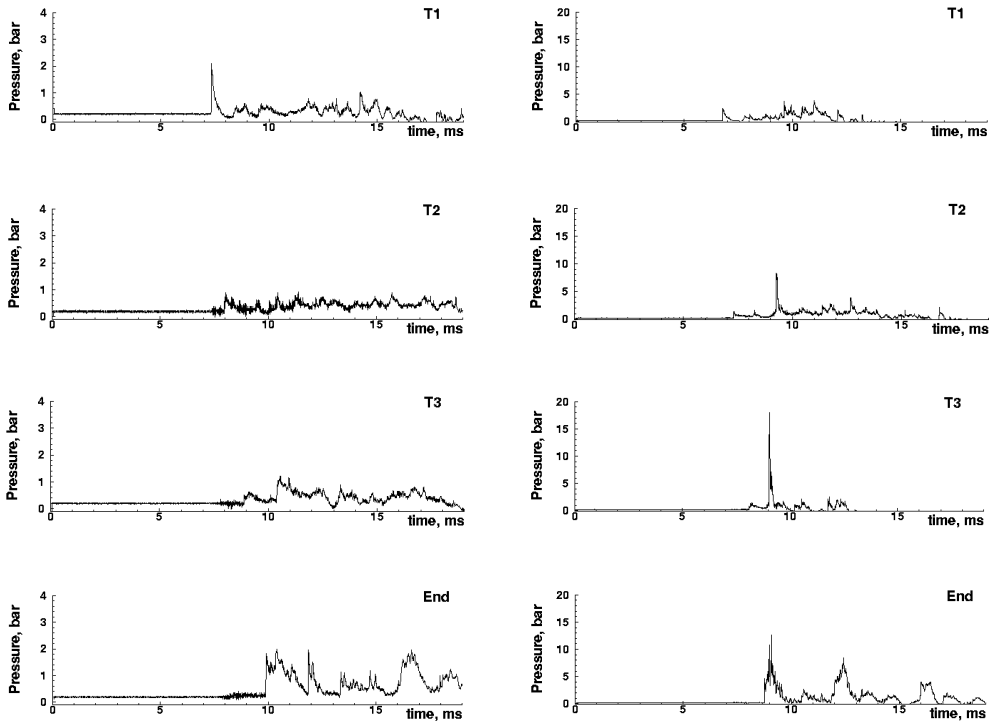

Figure 30: Pressure traces recorded along the receiver vessel wall and at the end wall for heterogeneous $C_{12}H_{26}$-O_2 mixtures. On the left, (shot 590) the initial temperature was 25 °C and only a decaying shock is observed. On the right, (shot 591) the initial temperature was 65 °C and a detonation is initiated on reflection. The two-port injection system was used in both cases. Note the difference in scale on the ordinate axes.

than required (around 150 ml), although the valve was only opened for the calculated injection time. This was so that the nozzles furthest downstream had sufficient fuel for the entire injection period. Since the valve could only be located outside the manifold, closing the valve did not immediately shut off the flow through the nozzles. However, since the mixture was ignited as soon as possible after the valve was closed, this did not introduce a significant error for this experiment. The manifold was not refilled or evacuated between tests. Pressure traces again show only the decaying driver shock.

The experiment was repeated with the manifold injection system at initial

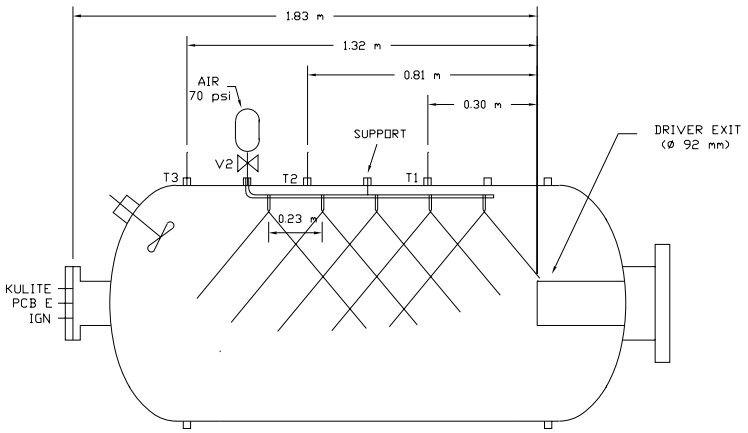

Figure 31: HYJET facility receiver vessel: manifold injection system configuration. (Driver vessel not shown.)

temperatures of 50°C (up to 10% of the fuel could vaporize if given sufficient time) and 65°C (up to 45% of the fuel could vaporize) and the results are shown in Fig. 32. No direct detonation was observed at 50°C, although a possible transition to detonation is observed between the end wall and T2. In the 65°C test, a pressure rise consistent with a detonation was observed on reflection from the end wall. Unlike the reflected initiation observed for the two-port injection system, in this case the detonation fails before reaching T3. The manifold injection time was shorter than for the two-port system, allowing less time for the fuel to vaporize. Also the two-port injection system was more likely to concentrate fuel in the downstream portion of the vessel.

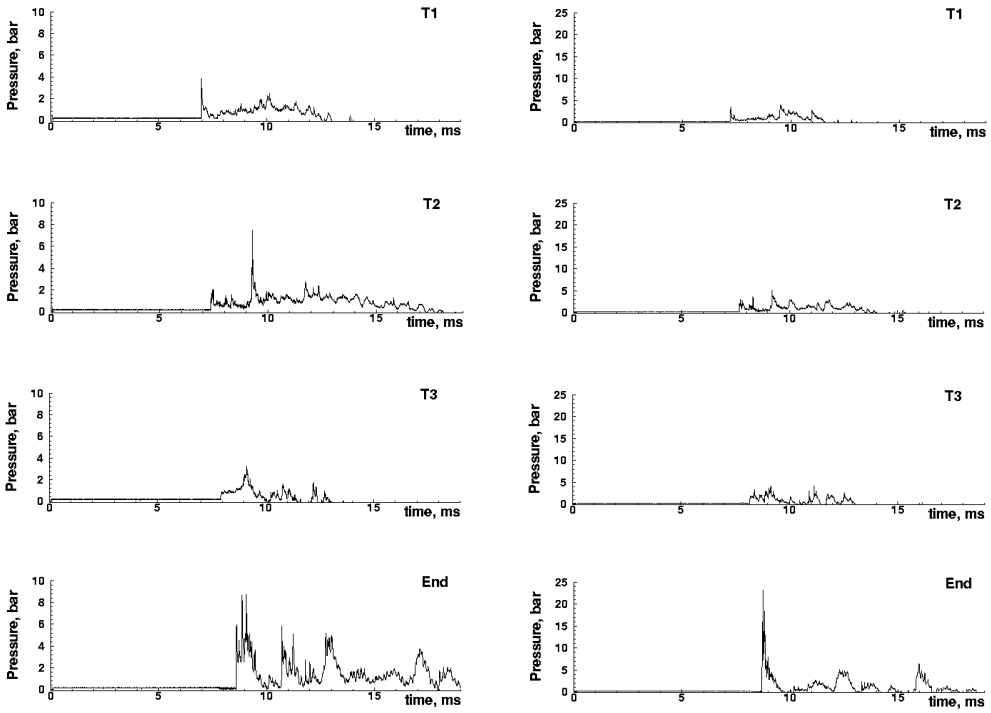

Figure 32: Pressure traces recorded along the receiver vessel wall and at the end wall for heterogeneous $C_{12}H_{26}$-O_2 mixtures. On the left, (shot 594) the initial temperature was 50 °C; on the right, (shot 595) the initial temperature was 65 °C. The manifold injection system was used in both cases. Note the difference in scale on the ordinate axes.

9 Summary and Conclusions

Detonations in C_6H_{14}-O_2-N_2 for different values of β were investigated, where β is the ratio of nitrogen to oxygen concentration.. Cell sizes varied from 1.7 mm for $\beta = 0$ to 51.1 mm for $\beta = 3.76$, corresponding to an estimated increase in the spherical critical initiation energy of four orders of magnitude. Comparison was made between similar β series studies for other fuels. C_6H_{14} cell widths are greater than those of H_2, C_2H_2 and C_2H_4, smaller than those of CH_4, and appear to be closest to C_3H_8.

CO is a principal intermediate product of hydrocarbon combustion yet there are relatively little cell width data available. A study was made of the effects of adding hydrogen or representative hydrocarbons to CO-air mixtures The greatest rate of reduction in cell width was due to addition of C_2H_2 and H_2, followed by C_2H_4, then C_6H_{14}. Detonations could be initiated in mixtures with very small fraction of C_6H_{14} (0.07% of the total mixture), and this detonation limit is thought to be dependant on the fraction of H atoms initially present in the mixture. Measured cell widths were compared with calculated reaction zone thicknesses. If the reaction zone thickness is taken to be defined by the location of the peak in OH concentration, the relationship was found to be approximately linear with slopes between 25 and 35 for the mixtures considered. Temperature and radical species profiles were calculated through the reaction zone with a ZND code. The measured cell width for all mixtures considered was found to be inversely proportional to the product of peak OH concentration and the CO concentration evaluated at that peak. peak: Command not found

This relationship was suggested by the dominant CO oxidation reaction in which oxidation occurs through the OH radical. Cell widths of mixtures containing H_2, C_2H_4, or C_6H_{14} could be collapsed on to a single line when plotted against this parameter. Cell widths for mixtures containing C_2H_2 showed a similar linear dependance on this parameter, but were a factor of two smaller than the cell widths for the other mixtures.

A significant decrease in cell width was measured for C_6H_{14}-air with the addition of low molecular weight fuels: H_2, C_2H_2, C_2H_4, in order of decreasing effectiveness. Cell widths measured for mixtures with 10 %(by fuel volume) addition of sensitizer are tabulated below (Table 3). Addition of 25% (by fuel mass) H_2 results in a 50% reduction in cell width and reduces the critical initiation energy (spherical source) to an eighth of that previously required. Addition of 10-75% by fuel mass of CO had little effect on the cell width, but

larger amounts increased the cell size, indicating the CO acts as an inhibitor. This result is supported by the above results which show the oxidation of CO proceeds much faster in the presence of hydrogen.

Sensitizer	H_2	C_2H_2	C_2H_4
Cell width (mm)	43.2	36.8	46.4

Table 3: Comparison of cell width measurements of C_6H_{14}-sensitizer-air mixtures with 10 % sensitizer addition (by fuel volume) at 100 kPa.

A hydrocarbon fuel blend representative of thermally decomposed JP-10 was studied at 295 K. Cell widths decrease from 27.6 mm for $\beta = 3.76$ to 1.0 mm for $\beta = 0$, corresponding to a decrease in initiation energy (spherical source) of four orders of magnitude. For a mixture composed of the JP-10 decomposition products, including the remaining O_2 and N_2, and sufficient air to make a stoichiometric mixture, the measured cell width was 55.8 mm. This is approximately the same as the cell width measured for stoichiometric C_6H_{14}-air, 51.1 mm, indicating the critical initiation energy is the same for both mixtures.

A jet-initiation facility was used to try to detonate both vapor phase and droplet phase mixtures of representative high vapor pressure hydrocarbons. The driver jet transitioned to detonation before entering the test section. Velocity measurements were made in vapor phase stoichiometric C_6H_{14}-O_2 and $C_{12}H_{26}$-O_2 mixtures with nitrogen dilution. The initial pressure was increased with increasing N_2 dilution to keep within the maximum design pressure of the facility. A critical nitrogen dilution limit, defined as the maximum β for which a detonation can be directly initiated in this facility, was found to be $2.5 \leq \beta \leq 3.0$ for both C_6H_{14}-$O_2$and $C_{12}H_{26}$ mixtures. For C_6H_{14} mixtures this corresponds to a D/λ (nozzle diameter/measured cell width) ratio of about 4 which compares well with the previously determined value of 4.3 (Krok 1997)for this facilty. There are no cell size data currently available for dodecane.

Two injection systems were tried in an attempt to detonate dodecane droplets. Nozzle spray parameters were known for water and were estimated for dodecane. The injection systems were tested with water outside the vessel, but the actual fuel injection could only be performed inside the vessel where the effect of droplets coalescing or adhering to the vessel walls could not be determined. These factors contributed to the uncertainty in characterizing

the initial mixture inside the vessel. The injection system tests outside the vessel indicated the largest source of error would be the fuel lost to the vessel walls, in particular to the bottom of the tank. A manifold injection system was designed to shorten the injection time to try to increase the fraction of fuel that remained suspended, and to improve the fuel distribution throughout the vessel. Detonations through decane sprays have been studied previously (Papavassiliou et al. 1992, Bowen et al. 1971, Bar-Or et al. 1982, Williams 1961) in continuous flow facilities. In these facilities, fuel droplets were produced by a nebulizer or by by agitating a fuel jet. The oxidant was seeded with the fuel particles and flowed continuously through a (usually vertical) tube. In this way, the initial mixture could be characterized.

It was hoped that increasing the initial temperature in the vessel might decrease the droplet size and so increase the settling time as well as increasing the amount of vapor in the surrounding mixture. It is not necessarily true, however, that smaller droplets are easier to detonate Papavassiliou et al. (1992), and self-sustaining detonations have been observed in decane sprays with particles of 2 - 400 μm (Papavassiliou et al. 1992, Bowen et al. 1971, Bar-Or et al. 1982, Williams 1961) and in diethylcyclohexane sprays with particles up to 2600 μm (Dabora et al. 1969). In a theoretical study, Williams (1961) calculated that if vaporization is the only mechanism present, the reaction zone for 30μm particles is 100 cm, making a detonation unlikely. However, Ranger and Nicholls (1969) determined that larger droplets could be shattered by the induced hydrodynamic flow around them and that this process could occur sufficiently rapidly for the shock and reaction zone to remain coupled. Borisov et al. (1970) considered vaporization, deformation, and shattering of droplets and concluded that vaporization was an adequate process for droplets of less than 10μm, droplet stripping was sufficient for droplets between 10 and 1000μm, while for larger droplets, local explosions around the droplets were necessary for sufficiently fast energy release.

References

Akbar, R. (1997). *Mach Reflection of Gaseous Detonations*. Ph. D. thesis.

Akbar, R., M. Kaneshige, E. Schultz, and J. Shepherd (1997). Detonations in H_2-N_2O-CH_4-NH_3-O_2-N_2 mixtures. Technical Report FM97-3, Graduate Aeronautical Laboratories: California Institute of Technology.

Bar-Or, R., M. Sichel, and J. Nicholls (1982). The reaction zone structure of cylindrical detonations in monodisperse sprays. *19th Symp. (Int.) Combust.*, 665–673.

Beeson, H., R. McClenagan, C. Bishop, F. Benz, W. Pitz, C. Westbrook, and J. Lee (1991). Detonability of hydrocarbon fuels in air. *Prog. Astronaut. Aeronaut 133*(19-34).

BETE nozzle company. *Manual no.104.3*. BETE nozzle company.

Bezmelnitsin, A., S. Dorofeev, and Y. Yankin (1997). Direct comparison of detonation initiation by turbulent jet under confined and unconfined conditions. Technical report, Russian Research Centre Kurchatov Institute, Moscow, Russia.

Borisov, A., B. Gelfand, S. Gubin, S. Kogarko, and A. Podgrebenkov (1970). The reaction zone of two-phase detonations. *Astronaut. Acta 15*, 411–417.

Bowen, J., K. Ragland, F. Steffes, and T. Loflin (1971). Heterogenous detonation supported by fuel fogs or films. *13th Symp. (Int.) Combust.*, 1131–1139.

Brabbs, T. and S. Merritt (1993). Fuel-rich catalytic combustion of a high density fuel. Technical Report 3281, NASA.

Burcat, A., E. Olchanski, and C. Sokolinski (1996). Kinematics of hexane combustion in a shock tube. *Israel Journal of Chemistry 36*, 313–320.

Carnasciali, F., J. Lee, R. Knystautas, and F.Fineschi (1991). Turbulent jet initiation of detonation. *Combust. Flame 84*, 170–180.

Curran, H., P. Gaffuri, W. Pitz, and C. Westbrook (1998). A comprehensive modelling study of n-heptane oxidation. *Combust. Flame 114*, 149–177.

Dabora, E., K. Ragland, and J. Nicholls (1969). Drop-size effects in spray detonations. *12th Symp. (Int.) Combust.*, 19–27.

Davidson, D., D. Horning, and R. Hanson (1999). Shock tube ignition time measurements for n-heptane/ O_2/Ar and JP-10/ O_2/Ar mixtures. *AIAA* (99-2216).

Dean, A., D. Steiner, and E. Wang (1978). A shock tube study of $H_2/O_2/CO/Ar$ and $H_2/N_2O/CO/Ar$ systems: measurement of the rate constant for $H+N_2O = N_2+OH^*$. *Combust. Flame 32*, 73–83.

Dixon, H. (1896). *Trans. Chem. Soc*, 759.

Gardiner, W. (1984). *Combustion Chemistry*. Springer-Verlag.

Kee, R., F. Rupley, and J. Miller (1989). Chemkin II: A fortran chemical kinetics package for the analysis of gas-phase chemical kinetics. Technical Report SAND89-8009, Sandia National Laboratory.

Kistiakowsky, G., H. Knight, and M. Malin (1952). Gaseous detonations. V. nonsteady waves in CO-O_2 mixtures. *J. Chem. Phys. 20*(6), 994–1000.

Knystautas, R., J. Lee, and C.M.Guirao (1982). The critical tube diameter for detonation failure in hydrocarbon-air mixtures. *Combust. Flame 48*(1), 63–83.

Krok, J. C. (1997). *Jet initiation of deflagration and detonation*. Ph. D. thesis, California Institute of Technology.

Lee, J., R. Knystautas, and C. Guirao (1982). The link between cell size, critical tube diameter, initiation energy and detonability limits. In *Fuel Air Explosions*, pp. 157–187. University of Waterloo Press.

Moen, I., J. Funk, S. Ward, G. Rude, and P. Thibault (1984). Detonation length scales for fuel-air explosions. *Prog. Aeronaut. Astronaut. 94*, 55–79.

Murray, S. and J. Lee (1986). The influence of physical boundaries on gaseous detonation waves. *Prog. Astronaut. Aeronaut. 106*(329-355).

Papavassiliou, J., A. Makris, R. Knystautas, J. Lee, C. Westbrook, and W. Pitz (1992). Measurements of cell structure in spray detonation. *Prog. Astronaut. Aeronaut. 154*, 148–169.

Pfahl, U. and J. Shepherd (1999). Jet initiation of deflagration and detonation in stoichiometric H_2-O_2-N_2 mixtures. Technical Report FM99-1, Graduate Aeronautical Laboratories, Califonia Institute of Technology.

Ranger, A. and J. Nicholls (1969). Aerodynamic shattering of liquid drops. *AIAA J. 7*, 285–290.

Reynolds, W. (1986, January). The element potential for chemical equilibrium analysis: implementation in the interactive program STANJAN. Technical Report A-3991, Dept. of Mechanical Engineering, Stanford University, Stanford, CA.

Schultz, E. and J. Shepherd (2000). Validation of detailed reaction mechanisms for detonation simulation. Technical Report FM99-5, Graduate Aeronautical Laboratories: California Institute of Technology.

Shepherd, J. (1986). The chemical kinetics of hydrogen-air-diluent detonations. *Prog. Astronaut. Aeronaut. 106*, 263–293.

Tieszen, S., D. Stamps, C. Westbrook, and W. Pitz (1991). Gaseous hydrocarbon-air detonations. *Combust. Flame 84*, 376–390.

Warnatz, J. and V. Karbach (1997). C2 mechanism for methane-air combustion. *http://www.ca.sandia.gov/tdf/3rdWorkshop/ch4mech.html*.

Westbrook, C. (1982). Chemical kinetics of hydrocarbon oxidation in gaseous detonations. *Combust. Flame 46*, 191–210.

White, D. and G. Moore (1965). Structure of gaseous detonation IV. induction zone studies in H_2 - O_2 and CO-O_2 mixtures. *10th Symp. (Int.) Combust.*, 785–795.

Williams, F. (1961). Structure of detonations in dilute sprays. *Phys. Fluids 4*(11), 1434–1443.

A Tables of experimental conditions and results

Table 4: GDT cell width measurements: hexane dilution series.

Shot no.	Mixture	P_o (kPa)	U_{CJ} (m/s)	U (m/s) 1-2	U (m/s) 2-3	λ_{av} (mm)
932	C_6H_{14}+9.5O_2	40	2313.6	2307.7	2303.9	1.7
933	C_6H_{14}+9.5(O_2+0.75N_2)	40	2104.6	2108.3	2107.1	6.3
934	C_6H_{14}+9.5(O_2+1.5N_2)	40	1987.4	2008.8	2006.5	16.0
935	C_6H_{14}+9.5(O_2+2.25N_2)	40	1904.6	1914.2	1911.2	30.4
936	C_6H_{14}+9.5(O_2+3.0N_2)	40	1839.2	1842.9	1842.6	50.5
937	C_6H_{14}+9.5(O_2+3.76N_2)	40	1783.0	1769.8	1758.6	91.7
940	C_6H_{14}+9.5(O_2+0.75N_2)	55	2116.0	2091.4	2088.0	6.1
939	C_6H_{14}+9.5(O_2+1.5N_2)	70	2004.3	2042.4	2002.2	8.3
941	C_6H_{14}+9.5(O_2+2.25N_2)	80	1922.0	1910.2	1909.2	19.7
942	C_6H_{14}+9.5(O_2+3.0N_2)	90	1857.9	1852.2	1850.0	23.7
938	C_6H_{14}+9.5(O_2+3.76N_2)	100	1800.5	1806.5	1797.9	51.1

Table 5: GDT cell width measurements: hexane sensitization series.'Air'=O_2+3.76N_2

Shot no.	Mixture	P_o (kPa)	U_{CJ} (m/s)	U (m/s) 1-2	U (m/s) 2-3	λ_{av} (mm)
938	C_6H_{14}+9.5Air	100	1800.5	1806.5	1797.9	51.1
951	0.95C_6H_{14}+0.05H_2+9.05Air	100	1800.0	1804.7	1801.4	39.2
945	0.9C_6H_{14}+0.1H_2+8.6Air	100	1800.5	1802.0	1804.9	43.2
950	0.8C_6H_{14}+0.2H_2+7.7Air	100	1801.3	1808.3	1801.4	42.7
947	0.7C_6H_{14}+0.3H_2+6.8Air	100	1803.3	1810.1	1804.9	39.5
965	0.6C_6H_{14}+0.4H_2+5.9Air	100	1805.3	1811.9	1806.6	38.5
948	0.5C_6H_{14}+0.5H_2+5.0Air	100	1807.8	1810.1	1803.1	34.9
993	0.1C_6H_{14}+0.9H_2+1.4Air	100	1853.0	1863.5	1857.4	27.3
994	0.05C_6H_{14}+0.95H_2+0.95Air	100	1884.0	1890.5	1887.8	21.9
995	0.02C_6H_{14}+0.98H_2+0.68Air	100	1932.4	1925.1	1922.7	13.5
996	0.01C_6H_{14}+0.99H_2+0.59Air	100	1943.6	1955.1	1947.4	10.1
880	H_2+0.5Air	100	1971.9	1985.0	1977.0	10.9
982	0.9C_6H_{14}+0.1C_2H_2+8.8Air	100	1801.5	1804.7	1804.9	36.8
985	0.7C_6H_{14}+0.3C_2H_2+7.4Air	100	1805.7	1810.1	1806.6	31.4
986	0.5C_6H_{14}+0.5C_2H_2+6.0Air	100	1813.1	1819.1	1810.2	32.2
987	0.3C_6H_{14}+0.7C_2H_2+4.6Air	100	1826.2	1833.7	1824.6	20.7
990	0.2C_6H_{14}+0.8C_2H_2+3.9Air	100	1835.4	1839.2	1835.3	14.1
998	0.1C_6H_{14}+0.9C_2H_2+3.2Air	100	1848.2	1856.0	1855.6	10.7
991	0.05C_6H_{14}+0.95C_2H_2+2.85Air	100	1856.7	1863.5	1857.4	8.4
992	C_2H_2+2.5Air	100	1867.5	1871.2	1866.8	6.2
967	0.9C_6H_{14}+0.1C_2H_4+8.85Air	100	1800.0	1808.3	1801.4	46.4
974	0.8C_6H_{14}+0.2C_2H_4+8.2Air	100	1801.5	1808.3	1803.1	35.3
966	0.7C_6H_{14}+0.3C_2H_4+7.55Air	100	1802.5	1804.7	1803.1	37.7
972	0.6C_6H_{14}+0.4C_2H_4+6.9Air	100	1804.2	1810.1	1799.6	35.8
968	0.5C_6H_{14}+0.5C_2H_4+6.25Air	100	1805.7	1792.4	1804.9	36.4
997	0.3C_6H_{14}+0.7C_2H_4+4.95Air	100	1809.8	1815.5	1815.5	24.7
1000	0.2C_6H_{14}+0.8C_2H_4+4.3Air	100	1813.5	1822.7	1819.1	24.7
998	0.1C_6H_{14}+0.9C_2H_4+3.65Air	100	1818.4	1830.0	1817.3	20.6
1001	0.05C_6H_{14}+0.95C_2H_4+3.33Air	100	1821.5	1833.7	1822.7	19.2
999	0.02C_6H_{14}+0.98C_2H_4+3.13Air	100	1823.8	1835.5	1828.1	17.0
899	C_2H_4+3Air	100	1825.0	1833.7	1829.9	22.8

Table 6: GDT cell width measurements: CO mixtures.'Air'=O_2+3.76N_2.(*: cells unreadable)

Shot no.	Mixture	P_o (kPa)	U_{CJ} (m/s)	U (m/s) 1-2	U (m/s) 2-3	$\lambda_a v$ (mm)
1058	9.5CO+0.5H_2+5O_2	100	1820.4	1830.0	1824.5	5.0
1057	9.5CO+0.5H_2+5(O_2+1.5N_2)	100	1754.6	1763.0	1761.9	12.5
1056	9.5CO+0.5H_2+5Air	100	1679.9	1683.5	1678.8	48.4
1118	0.995CO+0.005H_2+0.5Air	100	1671.4	859.2	766.0	no det.
1119	0.99CO+0.01H_2+0.5Air	100	1672.1	899.7	782.6	no det.
1151	0.99CO+0.01H_2+0.5Air	100	1672.1	1688.2	1669.7	det*
1152	0.99CO+0.01H_2+0.5Air	100	1672.1	562.0	534.1	no det.
1055	0.98CO+0.02H_2+0.5Air	100	1673.9	1671.2	1674.2	100.3
1056	0.95CO+0.05H_2+0.5Air	100	1679.9	1683.5	1678.8	48.4
1120	0.9CO+0.1H_2+0.5Air	100	1690.7	1699.2	1688.0	32
1150	0.7CO+0.3H_2+0.5Air	100	1739.2	1742.9	1745.3	16.9
1157	0.995CO+0.005C_2H_2+0.51Air	100	1674.0	915.9	812.5	no det.
1158	0.995CO+0.005C_2H_2+0.51Air	100	1674.0	1761.3	1678.8	102.3
1156	0.99CO+0.01C_2H_2+0.52Air	100	1677.2	1741.2	1677.2	90.5
1159	0.98CO+0.02C_2H_2+0.54Air	100	1683.7	1683.5	1681.8	49.5
1160	0.95CO+0.05C_2H_2+0.6Air	100	1701.5	1703.9	1701.9	29.9
1161	0.8CO+0.2C_2H_2+0.9Air	100	1763.7	1771.5	1768.6	10.9
1148	0.995CO+0.005C_2H_4+0.513Air	100	1673.4	824.0	746.6	no det.
1162	0.995CO+0.005C_2H_4+0.513Air	100	1673.4	972.4	863.7	no det.
1147	0.99CO+0.01C_2H_4+0.525Air	100	1676.4	1682.0	1672.7	71.8
1154	0.99CO+0.01C_2H_4+0.525Air	100	1676.4	1687.0	1679.0	89.7
1146	0.98CO+0.02C_2H_4+0.55Air	100	1682.2	1682.0	1680.3	54.3
1125	0.97CO+0.03C_2H_4+0.575Air	100	1687.9	1691.3	1689.5	43.8
1124	0.95CO+0.05C_2H_4+0.625Air	100	1698.3	1705.5	1697.3	36.2
1145	0.9CO+0.1C_2H_4+0.75Air	100	1720.1	1724.8	1714.6	33.8
1149	0.7CO+0.3C_2H_4+1.25Air	100	1770.8	1781.9	1778.9	25.2
1167	0.997CO+0.003C_6H_{14}+0.527Air	100	1675.2	1671.2	1672.7	112.0
1166	0.995CO+0.005C_6H_{14}+0.545Air	100	1678.0	1665.2	1686.4	89.4
1165	0.992CO+0.008C_6H_{14}+0.572Air	100	1682.4	1683.5	1681.8	69.7
1011	0.99CO+0.01C_6H_{14}+0.59Air	100	1770.8	542.1	1778.9	no det.
1164	0.988CO+0.012C_6H_{14}+0.608Air	100	1688.0	1685.1	1686.4	61.8
1163	0.985CO+0.015C_6H_{14}+0.635Air	100	1691.8	1697.6	1689.5	58.3
1009	0.98CO+0.02C_6H_{14}+0.68Air	100	1697.8	1700.7	1692.6	52.2
1008	0.95CO+0.05C_6H_{14}+0.95Air	100	1724.0	1685.1	1729.0	43.1
1007	0.9CO+0.1C_6H_{14}+1.4Air	100	1747.6	1756.2	1748.6	40.0
1006	0.7CO+0.3C_6H_{14}+3.2Air	100	1779.5	1788.9	1782.3	36.7
1005	0.5CO+0.5C_6H_{14}+5.0Air	100	1789.2	1797.6	1796.1	34.3
1004	0.3CO+0.7C_6H_{14}+6.8Air	100	1793.9	1801.2	1792.6	36.9
1003	0.1CO+0.9C_6H_{14}+8.6Air	100	1796.7	1806.5	1803.1	35.1

Shot	Mixture Fractions								Pressure	β	λ_{av}
no.	H_2	CO	CH_4	C_2H_2	C_2H_4	C_6H_{14}	O_2	N_2	(kPa)		(mm)
1060	0.025	0.046	0.009	0.002	0.013	0.009	0.188	0.707	100	3.76	27.6
1061	0.03	0.053	0.011	0.003	0.015	0.011	0.219	0.658	100	3.0	15.5
1062	0.035	0.064	0.013	0.003	0.018	0.013	0.262	0.591	90	2.25	10.6
1066	0.044	0.080	0.016	0.004	0.023	0.016	0.327	0.490	85	1.5	6.4
1065	0.058	0.105	0.021	0.005	0.030	0.022	0.433	0.345	75	0.75	2.9
1064	0.087	0.157	0.031	0.007	0.045	0.032	0.641	0.0	65	0.0	1.5
1067	0.021	0.039	0.007	0.002	0.008	0.008	0.161	0.751	100	4.66	55.8

Table 7: Composition of HCS mixtures.

Table 8: Hexane vapor phase experiments. Calculated fuel volume: 135 ml. Cell widths are interpolated from experiments performed at initial pressures from 40 kPa to 100 kPa (TableA).

Shot no.	β	T_o (C)	P_o (mbar)	Vol. fuel injected (ml)	U_{CJ} (m/s)	P_{CJ} (MPa)	P_{REF} (MPa)	U (m/s) T1-T2	U (m/s) T2-T3	P_{PEAK} (MPa) T1	P_{PEAK} (MPa) T2	P_{PEAK} (MPa) T3	λ (mm)
566	0	22.8	227	136	2278	0.83	2.09	2830	2478	1.53	1.30	1.25	3
567	0.75	24.1	381	142	2096	1.09	2.75	2873	2303	2.34	1.74	1.64	6.6
568	1.5	27.3	533	142	1998	1.31	3.26	2713	2670	2.87	2.13	2.06	11.9
569	2.25	25.4	690	149	1915	1.54	3.80	2560	2128	2.04	2.41	2.29	23
572	2.5	26.3	742	141	1896	1.65	4.07	2350	2161	3.64	2.36	2.34	-
570	3.0	27.6	844	139	1853	1.72	4.22	624	465	0.42	0.19	0.17	25.6
571	3.0	23.4	844	166	1853	1.72	4.22	581	443	0.38	0.19	0.15	25.6
573	3.76		1000	135	1797	1.88	4.62	572	441	0.35	0.2	0.16	51.1

Table 9: Dodecane vapor phase experiments. Calculated fuel volume: 92 ml

Shot no.	β	T_o (C)	P_o (mbar)	Vol. fuel injected (ml)	U_{CJ} (m/s)	P_{CJ} (MPa)	P_{REF} (MPa)	U (m/s) T1-T2	U (m/s) T2-T3	P_{PEAK} (MPa) T1	P_{PEAK} (MPa) T2	P_{PEAK} (MPa) T3
574	0.75	107.8	375	104	2078	0.84	2.07	2645	2191	2.34	1.11	1.02
575	1.5	107.6	531	122	1976	1.02	2.50	2558	2129	3.57	1.52	1.47
576	2.25	106.8	686	132	1901	1.18	2.88	1967	1964	1.56	1.71	1.76
578	2.25	105.7	686	149	1901	1.18	2.88	2397	2073	1.89	2.24	1.42
580	2.5	113.9	738	106	1882	1.30	3.18	2324	2018	2.90	1.96	1.70
581	2.5	107.5	738	112	1882	1.30	3.18	2397	2018	2.12	2.19	1.89
579	3.0	107.1	842	149	1843	1.40	3.40	697	522	0.45	0.21	0.15
582	3.0	106.9	842	112	1843	1.40	3.40	711	540	0.59	0.26	0.18